Chapter 5

Transducers, Beam Patterns, and Resolution

5.1 INTRODUCTION

A key ingredient of any ultrasonic instrument is the means for generating and detecting the acoustic waves. Since the origin of most generator signals is electrical in nature and since the most convenient way of conditioning, amplifying, and displaying signals is by electronic circuits, some device for translating electrical power into acoustical power, and vice versa, is needed. Among the possibilities are induction coil loudspeakers and magnetostrictive devices, but by far the most convenient transducers at ultrasonic frequencies are piezoelectric crystals and ceramics.

Piezoelectric materials (piezo = pressure) possess the property that a voltage applied to them will produce a pressure field on the atoms in their lattice (a stress) with an accompanying overall contraction or expansion in one or more dimensions of the material (a strain). The stress is a result of the lack of a center of inversion symmetry in the ionic lattice structure of the material; Figure 5.1 shows how an asymmetric atomic structure will distort in an applied electric field. By the piezoelectric property of the material, electrical excitation is changed into motion and pressure, the necessary elements for acoustic waves. Since the process is reversible, a piezoelectric crystal will also change an impinging pressure field into a strain and resulting voltage, so it can be used as an ultrasonic receiver just as well. Certain semicrystalline polymers, such as poly(vinylidene fluoride), PVDF, may also be made piezoelectric by stretching and polarizing them in a strong electric field during fabrication.

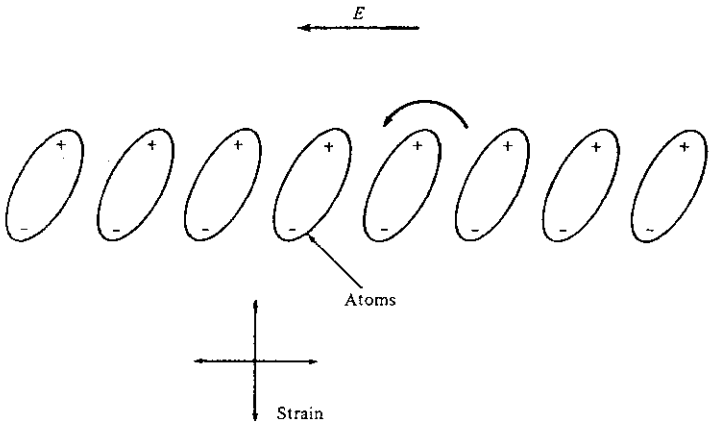

Figure 5.1 When an electric field E is applied to a piezoelectric material, in which charge asymmetry exists on an atomic scale, stresses and strains result in the material. This diagram is highly simplified.

In this chapter we discuss the details of electrical stimulation of piezoelectric transducers, analyze the spatial beam patterns from single transducers, and introduce the concept of multiple-element transducer arrays. It will be shown that the ultimate resolution (lateral and axial) of bioinstruments is determined by the size, frequency, and acoustical "Q" of the transducer used.

5.2 ELECTRICAL EXCITATION OF PIEZOELECTRIC TRANSDUCERS

Figure 5.2a shows a simplified diagram of a piezoelectric material cut and oriented for use as an ultrasonic transducer. The material might be quartz, barium titanate, lead zirconium titanate (PZT), or poly(vinylidene fluoride) (PVDF). Two opposite faces of the transducer are plated with conductive metal films; a voltage generator V is attached to the electrodes to produce an electric field E_z across the thickness l of the transducer whose magnitude is given by (assuming the diameter is much larger than l)

$$E_z = \frac{V}{l} \tag{5.1}$$

In piezoelectric materials in general, any given orientation of the electric field might produce two stresses (shear and compressional) in any of the three directions of the crystal, so a complete specification of the piezoelectric properties of the crystal would require a 3×6 tensor to tell

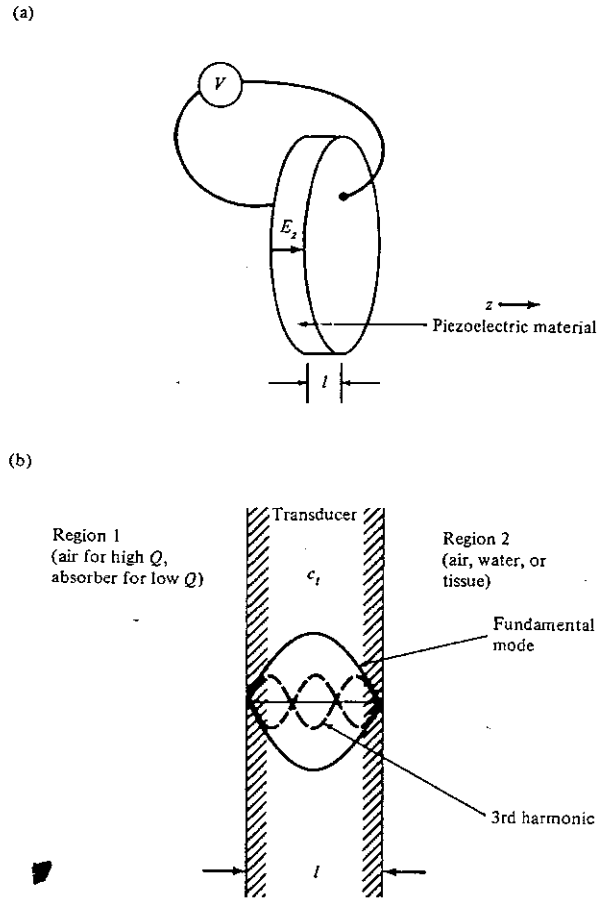

Figure 5.2 (a) Simplified sketch of a piezoelectric material used as a transducer with opposing electrodes. (b) In order to match excitation and boundary conditions, an odd number of half-wavelengths must fit between the transducer faces.

how each of the six components of the stress is related to each of the three components of the electric field. However, in practice the material is usually oriented to take advantage of the largest piezoelectric coefficient, which for most materials is one for which compressional stress is in the same direction as the applied electric field along some preferred axis. For the orientation shown in Figure 5.2a, known as the "thickness" mode of vibration, the pressure on the broad faces will be mainly longitudinal and the resulting pistonlike action will set up the desired compressional waves. The piezoelectric coefficient relating the resultant stress to the electric field

in this case is labeled as either e_{11} or e_{33}, depending upon the convention used for the particular crystal or ceramic.

There are two interesting possibilities for the temporal nature of the electrical excitation to the transducer—continuous wave (cw) and pulsed. These two cases are covered in order next.

5.2.1 Continuous Wave Excitation

If the voltage generator applies a voltage across the transducer of the form $V = V_0 \cos \omega t$, then the pressure waves produced will be continuous sinusoidal-type waves of the nature discussed in earlier chapters. These waves will propagate inside the crystal with a phase velocity c_t and will strike the front and back faces of the crystal. Here, they will be reflected in proportion to the impedance mismatch between the crystal material and the materials outside. Since the impedance of the transducer material is generally much higher than that of the air, water, or tissue media against the transducer faces, the reflection coefficient will be nearly $R = -1$, so the resultant pressure at the two boundaries must be nearly zero and a standing wave will be set up inside the transducer between its faces.

Only certain frequencies of excitation will be effective in generating waves that have the proper wavelength inside the transducer to match the simultaneous requirements for zero pressure at both interfaces. These frequencies, called the resonant frequencies of the transducer, are those for which an integral number of half-wavelengths fit between the faces of the transducer cavity. In addition, because the electrical excitation has the same polarity across the entire thickness of the transducer at any given instant (since electrical wavelength is much larger than l), only standing wave patterns with an odd number of half-wavelengths will be efficiently driven by the electrical input. Patterns with an even number of half-wavelengths will always have an equal number of regions with opposite phases, which will cancel electrically, leading to minimal coupling with the input field.

Figure 5.2b shows two waves which match both the boundary conditions and the excitation requirement. The lowest frequency to satisfy the resonance condition is called the fundamental frequency of the crystal, and at this frequency a single half-wavelength fits inside the cavity. The nulls of the pressure standing wave occur at the faces of the transducer to match the boundary conditions. For a transducer of thickness l, the fundamental frequency f_1 will have a wavelength λ_1 inside the transducer such that

$$\frac{\lambda_1}{2} = l \tag{5.2}$$

Since $\lambda_1 = c_t/f_1$, where c_t is the compressional wave velocity in the transducer material, then

$$\boxed{f_1 = \frac{c_t}{2l}} \tag{5.3}$$

At ultrasonic frequencies, the thickness required to use a transducer crystal in its fundamental mode can be quite thin, making some crystals fragile (see Problem 5.1), so very-high-frequency transducers are sometimes employed in their higher harmonic modes. As an example, Figure 5.2b shows a third harmonic wave which will oscillate at three times the frequency of the fundamental.

Frequency Response

Near each of the resonant frequencies, the transducer will have a response to voltage that will vary according to the proximity of its frequency to the resonant frequency. A curve showing how the power density I radiated by a transducer varies as a function of frequency around its point of resonance is given in Figure 5.3. The narrowness or broadness of the resonance curve, as measured by the frequency width Δf to the half-power points, is defined by the so-called quality factor, or Q, of the cavity in the following way:

$$\frac{f_1}{\Delta f} = Q \tag{5.4}$$

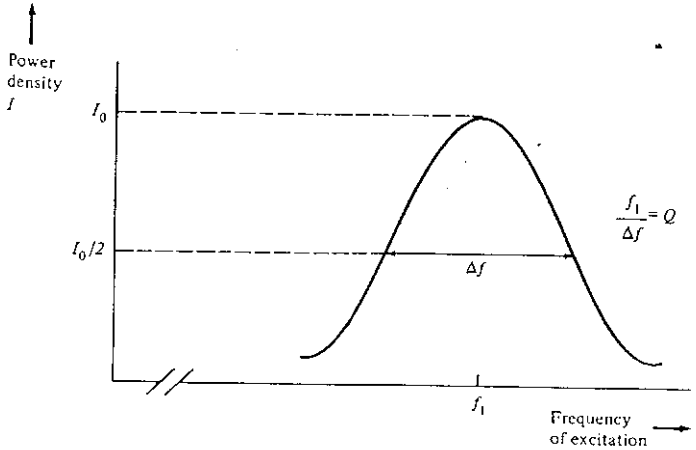

Figure 5.3 The resonance curve for a transducer with center frequency f_1 and quality factor Q. The larger Q, the narrower the frequency response.

Thus, a high Q leads to a very narrowly peaked resonance, and a low-Q transducer has a broadband response.

The magnitude of Q is determined by the losses (absorption and transmission) encountered in the transducer. By far the largest contributor to the losses of most transducers is the transmission of acoustic power through the faces into neighboring regions, since the internal loss of good transducer materials, especially quartz, is small. If air forms the regions on both sides of the transducer, the impedance mismatch is so large that hardly any power escapes, leading to Q values as high as 30,000. In fact, for use in high-precision frequency oscillators, quartz crystals are mounted in small evacuated cans where the vacuum environment gives very low transmission losses with Q values approaching 1,000,000. Since Δf is so small for these crystals, they are in common use in electronic equipment whenever accurate frequencies are needed, as in quartz watches.

Of course, if the transducer is to be used for radiating acoustic waves into tissues, some power is purposely lost through one face of the transducer. When tissue replaces air at one of the transducer faces, the impedance mismatch is reduced, power is transmitted, and the Q of the cavity goes down dramatically.* Problem 5.7 shows that for a typical rigid crystal transducer such as quartz radiating into tissue, $Q \approx 5$–15.

Since air presents a large impedance mismatch with the transducer (as compared to tissue), no air can be allowed to find its way between the transducer face and the tissue surface being irradiated if maximum power transmission into tissue is desired. Any air layer more than a fraction of a wavelength in thickness will reflect considerable power back into the transducer, reducing its effectiveness as a transmitter. Thus, in clinical practice, mineral oil or commercially available gel is used to coat the transducer and force out any air between the transducer/tissue interface.

Radiated Power

The power density that a transducer driven by a voltage source will radiate into a medium may be found by using the piezoelectric relationship for the transducer:

$$p_i = e_{ii}E_i - c_{ii}\left(\frac{\partial \xi}{\partial z}\right) \tag{5.5}$$

where

p_i is the pressure in the transducer material

E_i is the electric field applied

* The resonant frequency of the transducer is also slightly lowered from its lossless value, because of the loss now encountered.

e_{ii} is the material's piezoelectric stress coefficient

ξ is the displacement of the particles in the material, so $\partial \xi/\partial z$ is strain (elongation or compression) of the material

c_{ii} is the elastic stiffness constant of the material

i is a subscript denoting the directions of the pressure, electric field, and strain (here assumed to be all in the same direction).

The analysis then assumes two countertraveling acoustic waves inside the transducer, as diagrammed in Figure 5.4. When combined, these two waves produce the standing wave pattern described earlier. By matching boundary conditions at the two faces for continuity of both pressure and velocity across the interfaces, similar to the procedure of Section 3.4.2, and using Equation (5.5), it can be shown (see Problem 5.3) that the velocity of the transducer faces at resonance is

$$u_f = \pm \frac{2e_{ii}E_i}{Z_1 + Z_2} \tag{5.6}$$

where Z_1 and Z_2 are the acoustic impedances of the media on either side of the transducer, and the $\pm$ sign denotes that the face velocities are in opposite directions since a resonant vibration mode with an odd number of half-wavelengths was assumed.

Many transducers have air in the region to the rear; for this case, $Z_1 \approx 0$ and Equation (5.6) gives the velocity of the front face (touching tissue or water) as

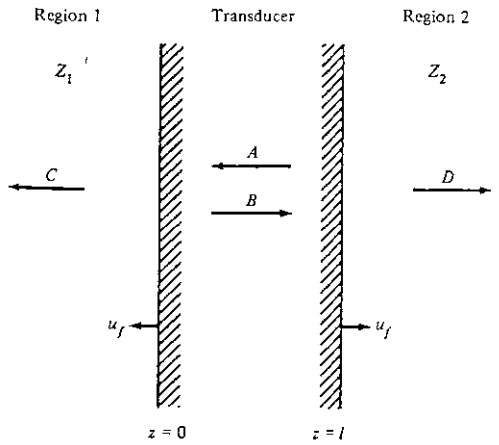

Figure 5.4 Analysis of waves excited inside a transducer. Matching the velocity and pressure boundary conditions at the two faces leads to Equation (5.6).

$$u_f = \frac{2e_{ii}E_i}{Z_2} \tag{5.7}$$

The power density transmitted forward into medium 2 is then easily found from velocity continuity and the relationship $I = Zu^2$ to be

$$I = \frac{4e_{ii}^2 E_i^2}{Z_2} \tag{5.8}$$

For the configuration shown in Figure 5.2a where the transducer is excited by a sinusoidal voltage source, Equation (5.1) may be used to give the average radiated power density:

$$I_{\text{ave}} = \frac{2e_{ii}^2 V_0^2}{l^2 Z_2} \tag{5.9}$$

where V_0 is the peak sinusoidal exciting voltage and a factor of $\frac{1}{2}$ was used to give the time average of power density.

Piezoelectric Coefficients

As Equation (5.9) shows, the ability of a transducer to convert voltage into acoustical power is related to the strength of its piezoelectric stress coefficient e_{ii}. Table 5.1 gives some values for various piezoelectric materials commonly used as ultrasound transducers. Sometimes the literature will list other related coefficients, such as d_{ii}, the piezoelectric strain coefficient (sometimes called the transmitting constant). It is related to e_{ii} by the relationship

$$e_{ii} = d_{ii}c_{ii} \tag{5.10}$$

where c_{ii} is the material's elastic stiffness constant (under conditions of constant electric field). Also, the piezoelectric coefficient g_{ii} (sometimes called the voltage output coefficient, or receiving constant) may be given. It is related to d_{ii} by

$$d_{ii} = g_{ii}\epsilon_r\epsilon_0 \tag{5.11}$$

where ϵ_r is the relative dielectric constant of the transducer material (under unrestrained or free conditions), and ϵ_0 is the permittivity of free space ($\epsilon_0 = 8.85 \times 10^{-12}$ F/m).

By scanning Table 5.1 it can be seen that there are large differences in e_{ii} and ϵ_r (and therefore in d_{ii} and g_{ii}) among the materials. It would appear that barium titanate or PZT are by far the most efficient radiators, and indeed they are widely used as good transducer materials. But the picture is more complicated than just comparing the values of e_{ii}, since other factors must be considered, such as the electrical coupling of the

TABLE 5.1 VALUES FOR SOME PIEZOELECTRIC TRANSDUCER MATERIALS

Material	Density ρ_0 (kg/m^3)	Elastic stiffness c_{ii} (N/m^2)	Phase velocity c_t (m/s)	Acoustic impedance Z_c (kg/m^2 s)	Relative dielectric constant ϵ_r	Piezoelectric stress coeff. e_{ii} (N/V m)
Quartz (x-cut)	2.7×10^3	86×10^9	5.8×10^3	15×10^6	4.5	.17
Barium titanate	5.7×10^3	110×10^9	5.3×10^3	30×10^6	1700	8.6
Lead zirconium titanate (PZT)	7.5×10^3	83×10^9	4.0×10^3	30×10^6	1200	9.2
Poly(vinylidene fluoride) (PVDF)	1.8×10^3	3×10^9	1.4×10^3	2.5×10^6	12	.069

transducer to the transmitting and receiving circuitry, the internal losses of the material, the material's phase velocity and dielectric constant, the temperature range allowable, and physical attributes such as flexibility and ease of fabrication. For example, for a fixed frequency of resonance, Equation (5.3) shows that a transducer's thickness l is proportional to the material's phase velocity c_t. Therefore, a transducer made from PVDF, because of its relatively low c_t, will be thinner than one of barium titanate. Consequently, since l^2 appears in the denominator of Equation (5.9) for output power, the electric field is high for a given voltage, and PVDF is not as weak as would be predicted by its low value of e_{ii} alone.

Equivalent Circuits of Transducers

Electrical characterization of the transducer is very important in determining the electrical load that the transducer presents to the drive or receiver circuitry and in optimizing the match between the two. As a step in finding the equivalent electrical circuit, a companion equation to Equation (5.5) gives the surface charge density σ_i appearing at the face of the transducer:

$$\sigma_i = \epsilon_r \epsilon_0 E_i - d_{ii} p_i \tag{5.12}$$

This surface charge, occurring on the two parallel electrodes separated by the thin piezoelectric material, forms the essence of a parallel-plate capacitor. The capacitance C_0 of such a parallel-plate capacitor is given by the well-known equation

$$C_0 = \frac{q}{V} = \frac{\sigma_i A}{E_i l} = \frac{\epsilon' A}{l} \tag{5.13}$$

where

q = total charge on either plate
V = voltage between plates
A = area of plate (transducer area)
l = spacing between plates
ϵ' = effective dielectric constant of material between plates.

Due to the piezoelectric activity of the transducer material represented by the second term on the right-hand side of Equation (5.12), the effective dielectric constant ϵ' of the material when used in a nonfree ($p \neq 0$) condition is different from its free value of $\epsilon_r \epsilon_0$. To determine ϵ' for an important nonfree situation, namely, when the transducer is clamped so that all strain is zero, Eq. (5.5) with $\partial \xi / \partial z = 0$ is substituted into Equation (5.12) for p_i:

$$\begin{aligned} \sigma_i &= \epsilon_r \epsilon_0 E_i - d_{ii} e_{ii} E_i = \epsilon_r \epsilon_0 \left(1 - \frac{d_{ii} e_{ii}}{\epsilon_0 \epsilon_r}\right) E_i \\ &= \epsilon_r \epsilon_0 (1 - g_{ii} e_{ii}) E_i \\ &= \epsilon_r \epsilon_0 (1 - \kappa^2) E_i \end{aligned} \tag{5.14}$$

where $\kappa = \sqrt{g_{ii} e_{ii}}$ is known as the coefficient of electromechanical coupling of the material. It can be shown that the parameter κ is related to the ratio of mechanical energy to electrical energy stored in the vibrating transducer.

Using Equation (5.14) in Equation (5.13) gives the material's effective dielectric constant ϵ' under clamped conditions:

$$\epsilon' = \epsilon_r \epsilon_0 (1 - \kappa^2) \tag{5.15}$$

and the capacitance of the transducer when clamped:

$$\boxed{C_0 = \epsilon_r \epsilon_0 (1 - \kappa^2) \frac{A}{l}} \tag{5.16}$$

A detailed electrical analysis of a transducer at resonance (see Problem 5.4) shows that the transducer appears electrically to be composed of just two elements: a capacitor of value C_0 given by Equation (5.16), which represents the accumulation of surface charge on the plates due to the applied voltage; and a parallel resistor R_m, which represents the transformation of electrical power into radiated acoustical power. The value of R_m, called the *motional resistance*, can easily be found from Equation (5.9) and the fact that, for this transducer with no assumed internal losses, all average electrical power $V_0^2/2R_m$ consumed must equal the average acoustical power $I_{ave} A$ radiated. Using Equation (5.9) in this equality,

$$\frac{2 e_{ii}^2 V_0^2 A}{l^2 Z_2} = \frac{V_0^2}{2 R_m}$$

or, solving for R_m,

$$\boxed{R_m = \frac{l^2 Z_2}{4 e_{ii}^2 A}} \tag{5.17}$$

Figure 5.5a shows the equivalent electrical circuit at resonance, with the values of C_0 and R_m given by Equations (5.16) and (5.17), respectively. The capacitance C_0 can be moderately high (due to the large values of ϵ_r for many transducer materials, as large as $\epsilon_r = 1700$ for barium titanate), and the resistance R_m is inversely proportional to the power radiated by the device; high acoustic radiating ability means a low value for the parallel R_m, and vice versa. Problem 5.5 gives values typical of a medical imaging transducer.

As the circuit of Figure 5.5a shows, a transducer appears capacitive in nature right at its frequency of resonance. So, to efficiently match it to the driving voltage generator, a parallel inductor L_0 is sometimes placed between the transducer and generator. The value of the inductor is chosen such that the electrical resonance frequency $\omega = \sqrt{1/L_0 C_0}$ is matched to the acoustical resonance frequency. A transformer may also be used to

(a)

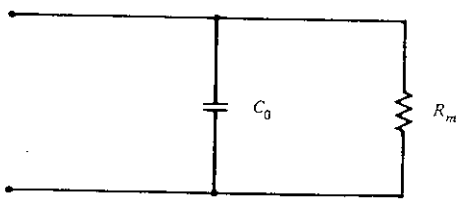

(b)

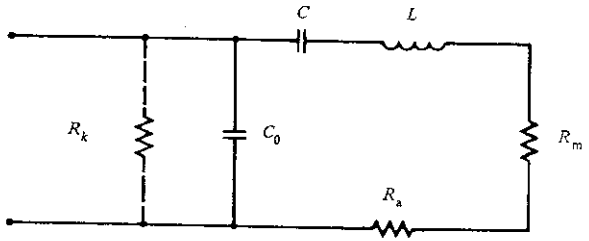

Figure 5.5 (a) The equivalent electrical circuit for a lossless transducer precisely at resonance. C_0 is the parallel-plate capacitance of the device (with a modified dielectric constant ϵ' to account for the piezoelectric activity), and R_m is a resistance representing the radiation of acoustic power. (b) The complete equivalent circuit in the neighborhood of resonance adds an inductance L and capacitance C in series with R_m. To complete the picture, possible internal loss resistances R_k and R_a may also be added. At resonance, the impedances of L and C cancel.

transform the transducer's resistance at resonance, R_m, to match the output impedance of the generator, usually 50 ohms. However, the addition of an electrical resonance circuit increases the overall electrical Q of the network, and in some applications, such as when short acoustic pulses are required for echo ranging, a high Q is not desirable; the effect of Q on pulse length is covered in the next section.

When the frequency driving the transducer is moved away from resonance, two more components are needed to characterize the equivalent circuit: an inductor L and a capacitor C in series with R_m. The impedance of these two elements cancel right at resonance but give this branch a capacitive nature below resonance and an inductive nature above resonance.

To complete the picture, two more resistors may be added to account for any nonradiative losses in the transducer: a parallel resistor R_k (generally large) to account for leakage current, and a series resistor R_a (generally small) to account for internal absorption in the material. Figure 5.5b shows the complete equivalent circuit, which is valid in the neighborhood of resonance as well as at resonance.

Comparison of Piezoelectric Materials

Returning now to Table 5.1, it can be noted that the top three materials listed in the table are fairly dense, rigid crystals. Quartz occurs both as a natural crystal or may be man-made (SiO_2). Barium titanate and PZT are man-made ceramics that are rendered piezoelectric by first heating above their Curie temperature, then cooling in the presence of a strong electric field to produce a permanent "ferroelectric" effect. These man-made materials may be molded during fabrication to the desired diameter and thickness; sometimes a concave face is molded into the tissue side of the transducer to give focusing of the radiated beam. Note that these three crystals have high acoustic impedances (compared to soft tissue impedance of about 1.5×10^6 kg/m^2 s) due to their dense and relatively incompressible nature.

The polymer transducer material PVDF is much softer and less dense than the other materials. As such, it may be fabricated as a film and has the possibility of being shaped around nonplanar body surfaces. It is fabricated by first stretching the raw material along one direction, then polarizing it in a strong dc electric field. The acoustic impedance of PVDF is a much closer match to that of tissue, and therefore more power is coupled out into the tissue. This lowers the Q of the transducer (see Problem 5.9), making it more broadband and giving it better axial resolution, as discussed in Section 5.2.2. Unfortunately, these advantages are offset somewhat by the larger internal loss that PVDF has compared to the crystalline or ceramic materials, by its lower temperature range of operation (restricted to below about 80°C for continuous exposure, which limits the amount of power it can handle as a transmitter due to heat generation by its internal loss), and by its generally lower piezoelectric transmission coefficients e_{ij} and d_{ij}.

When used in the receiver mode, though, the concern is not so much with the efficiency of the transducer in transforming electrical energy into acoustical energy. Rather, the receiver element is often connected to a high-input impedance voltage amplifier, and a good measure of receiving sensitivity is the voltage output coefficient $g_{ij} = d_{ij}/\epsilon_r\epsilon_0$. Due to the low relative dielectric constant of PVDF ($\epsilon_r = 12$), its voltage output coefficient is high, making it a better receiving material than an efficient energy transmitting element.

We now turn our attention to the other basic way of exciting ultrasonic transducers—with a sharp pulse of electrical voltage. This mode of operation is actually the most common for medical instrumentation, inasmuch as

the majority of these imagers use pulsed echoes to locate and image the deep-lying tissue boundaries within the body. The precision with which the boundaries are located along the direction of the beam travel (axial resolution) will be shown to be directly related to the time behavior of the transducer's response to the input voltage pulse, as characterized by the Q value of the transducer.

5.2.2 Pulsed Excitation and Axial Resolution

If the electrical input to the transducer is a sharp impulse of voltage, such as that obtained by rapidly discharging a capacitor using a circuit similar to that shown in Figure 5.6, the pressure wave radiated by the transducer will take the form of an exponentially decaying sinusoid. The voltage pulse may be either negative or positive with respect to ground; a negative pulse is often easier to generate with a positive supply using the circuit shown in Figure 5.6.

Figure 5.7 shows the example of a positive voltage pulse and the resultant pressure waveform from the transducer. The pressure waveform does not precisely duplicate the waveform of the voltage (i.e., a sharp pulse of pressure) because the crystal possesses resonant qualities as discussed in the previous section. When excited by an impulse, the crystal will resonate sinusoidally at its fundamental frequency; the envelope of this wave will decay at a rate proportional to the losses (internal and transmitted) of the

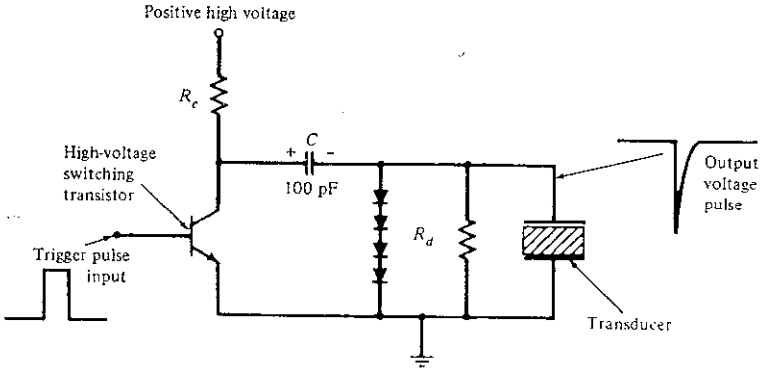

Figure 5.6 An electrical circuit for generating a sharp voltage pulse to a transducer. During the off-time of the transistor, the capacitor charges to the high supply voltage. When the transistor is turned on by the trigger pulse, its low on-resistance takes the left side of the capacitor to near ground voltage, applying a large negative pulse to the upper transducer terminal. The capacitor then discharges through the transducer. R_d is a damping resistor for shaping the trailing edge of the pulse.

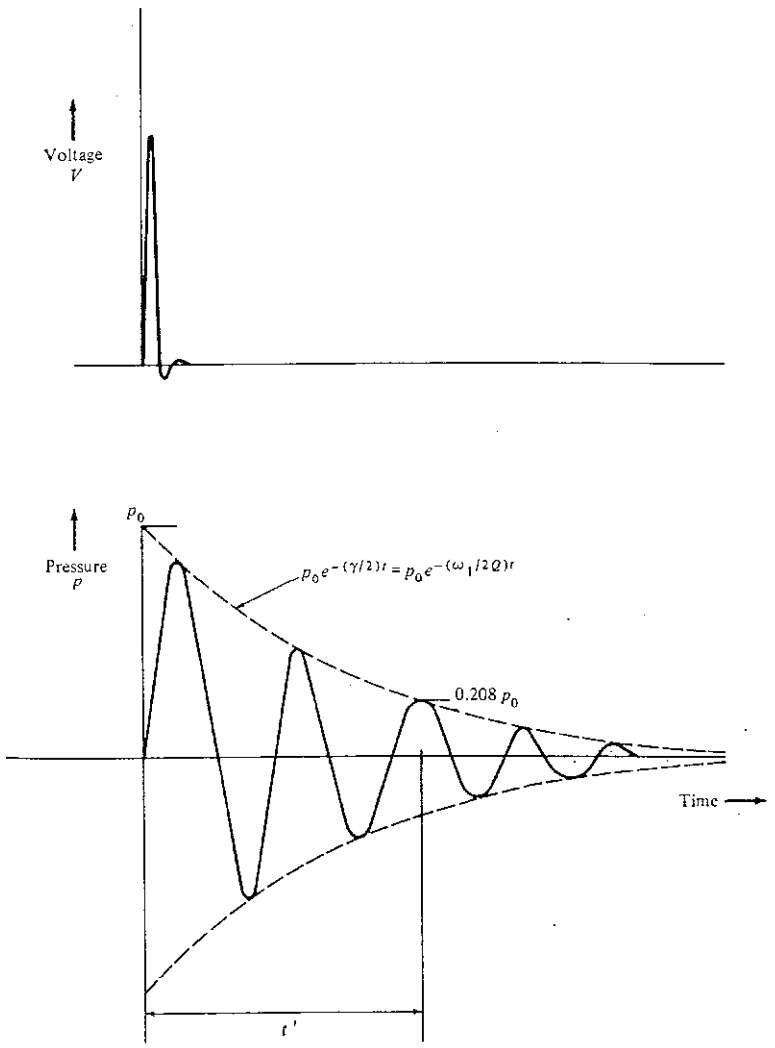

Figure 5.7 The pressure waveform radiated by a transducer excited by a sharp impulse of voltage. The pressure at any distance decays at a rate inversely proportional to the Q of the transducer. For the waveform of this figure, Q is approximately 4.5.

transducer. In a real sense, the crystal acts in the same fashion as a bell when struck a sharp blow by a hammer, except that the losses due to radiation from the ultrasonic transducer are much larger than those found in a good-quality bell, so the transducer will not "ring" as long.

The rate of decay is proportional to the losses in the transducer, so it is natural to expect that the rate will be related to the Q of the crystal. Indeed, a definition of Q that is entirely consistent with Equation (5.4) but is of a different form can be given in terms of the energy lost per cycle of resonance as follows:

$$Q = \frac{\text{energy stored}}{\text{energy lost per cycle}} 2\pi \tag{5.18}$$

If we let J represent the energy stored by the crystal, then Equation (5.18) can be rearranged in differential form as

$$\frac{dJ}{dt}\frac{1}{f_1} = -\frac{2\pi J}{Q} \tag{5.19}$$

where f_1 = frequency of resonance. The solution to Equation (5.19) has an exponential decay as a function of time:

$$J = J' e^{-\gamma t} \tag{5.20}$$

Substituting Equation (5.20) into Equation (5.19) and solving for γ yields the decay rate in terms of Q:

$$\gamma = \frac{2\pi f_1}{Q} = \frac{\omega_1}{Q} \tag{5.21}$$

Since the power output of the transducer is proportional to the energy stored in its oscillations, and since the magnitude of the radiated pressure wave is proportional to the square root of the power in the wave, it is possible to write the time decay of the envelope of the pressure wave radiating from a transducer with a given Q as

$$\boxed{p = p_0 e^{-(\gamma/2)t} = p_0 e^{-(\omega_1/2Q)t}} \tag{5.22}$$

where Equation (5.21) has been used to relate γ to the Q of the transducer. Thus, a high Q leads to a long ringing time whereas a low Q gives a shortened waveform. Figure 5.7 plots the pressure waveform for the example of a low-Q transducer.

As an approximate rule of thumb, it can be said that the number of cycles contained in the power waveform is roughly numerically equal to the Q of the transducer.* This can be shown by defining the point in time when the waveform is effectively ended to be that time t' when the power has diminished to $e^{-\pi} = 0.043$ of its original value and the pressure has

* As Problem 5.10 shows, "the Q of the transducer" is really not correct nomenclature since the value of Q is not a fixed characteristic of the transducer but is determined by the type of material against which the transducer is placed and will vary from application to application with the same transducer. However, in ultrasonic bioinstrumentation the transducer is invariably placed against tissue, so the resulting Q will be reasonable fixed.

therefore diminished to $e^{-\pi/2} = 0.208$. This point is shown on Figure 5.7. From Equation (5.22),

$$\frac{\omega_1}{2Q} t' = \frac{\pi}{2}$$

so

$$t' = \frac{2\pi Q}{2\omega_1} = \frac{Q}{2f_1} \tag{5.23}$$

Since the period of one cycle of the power waveform is one-half the period of the pressure waveform (see Figure 3.1) and the pressure period is given by $1/f_1$, the period of the power waveform is $1/2f_1$, and

$$\boxed{t' \approx Q \text{ periods of power}}$$

As the rule of thumb states, there are approximately Q cycles of power (and, correspondingly, $Q/2$ cycles of pressure) contained in the pulse.

Axial Resolution

An important design question is now appropriate: Is it desirable to have a high-Q or a low-Q transducer for bioinstruments? The answer depends upon whether the instrument is operated cw (as some Doppler flowmeters are) or pulsed (as in echocardiography). If cw, for efficiency's sake it is best that the transducer has as high a Q as the transmission at the tissue interface will allow. The voltage exciting the transducer should then be a continuous sine wave centered at the resonant frequency of the crystal as determined by its thickness.

If operated pulsed, however, a low-Q transducer is desirable. This is because the *axial resolution* (AR) of the instrument is dependent upon the length of the pulsed waveform. Since the depth of the boundaries being investigated by a pulsed instrument is determined by measuring the round-trip transit time of the pulses reflected from the boundaries, the more accurate this time can be measured, the more accurate will be the determination of depth. It is clear that a shorter transmitted pulse will lead to a more precise measurement of the time of arrival of the echoes and, in turn, the depth of the reflecting borders. If we define the effective pulse time to be t' as previously and use the straightforward relationship that distance equals the product of time and velocity, we get

$$\text{Axial resolution} \approx \frac{t'c}{2} \tag{5.24}$$

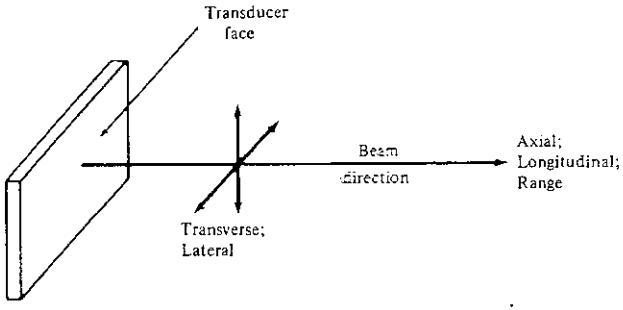

Figure 5.8 Conventions for directions related to beam propagation from a transducer.

where the factor of 2 enters because of the round-trip nature of the reflected wave (see Problem 5.6).

The nomenclature that is conventionally used to describe the directions related to a transducer and its propagating beam is summarized in Figure 5.8. Note that the terms "axial" and "longitudinal" are generally interchangeable, as are "transverse" and "lateral." Axial resolution pertains to spatial resolution in the direction of beam propagation, whereas transverse resolution is measured in the plane perpendicular to the beam's direction.

Seen in another way, axial resolution is a measurement of an instrument's ability to resolve two reflecting boundaries that are closely spaced in the axial (or longitudinal) direction of the instrument. Figure 5.9 shows the time sequence of pulses reflected from two closely spaced interfaces. It can be said that when the two boundaries are spaced apart in the longitudinal direction a distance equal to or greater than the axial resolution,* they can be resolved as separate reflectors. When they are closer, their echoes blend into one another.

Since the effective time length of a transducer's pulse is related to Q, Equation (5.24) for axial resolution can be rewritten using Equation (5.23):

$$\text{Axial resolution} \approx \frac{Qc}{4f_1}$$

Put in terms of wavelength,

$$\boxed{\Delta R \approx \frac{Q\lambda}{4}} \qquad (5.25)$$

* Some authors prefer defining resolution as the *inverse* of minimal resolvable distance, with units of cycles per mm. In this text, we will use distance directly, since this definition seems more straightforward. In any case, the units tell the definition.

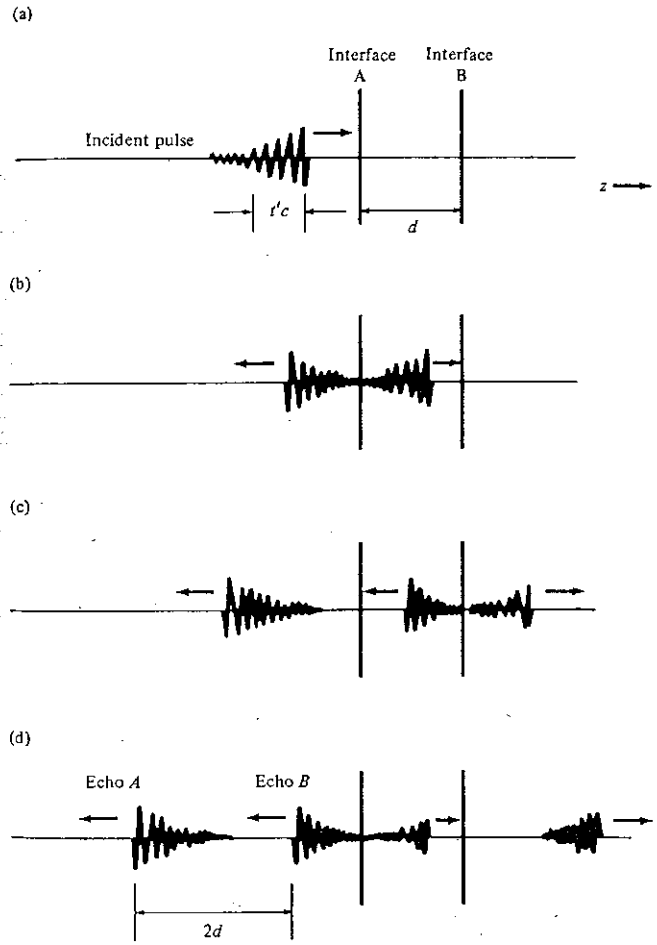

Figure 5.9 Four successive snapshots of the positions and lengths of echoes from two closely spaced interfaces. When d is reduced to the point where the echoes overlap but are just resolvable, then d = axial resolution.

which shows that improved resolution (a smaller value for Equation (5.25)) is a result of a lower-Q transducer. In fact, loss is sometimes purposely added to the back face of a transducer to lower its Q and improve its resolution. Although the total acoustic output power of the transducer (for a given electrical excitation) is reduced by this technique, the increased axial precision of imaging is often worth the cost. Figure 5.10 shows how

(a)

(b)

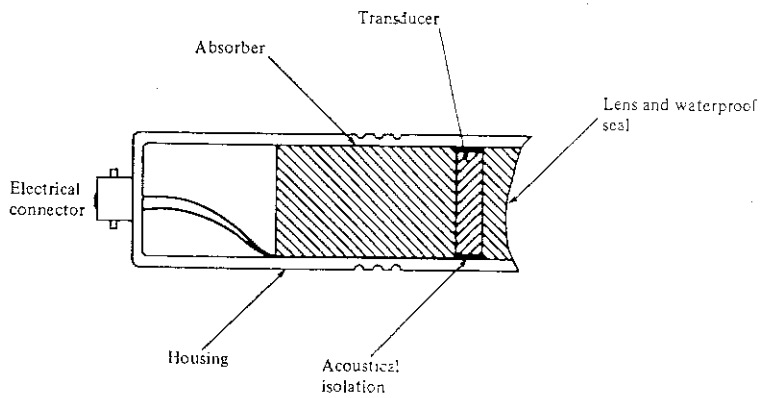

Figure 5.10 (a) A photo of a typical 3.5-MHz single element transducer. Its diameter is approximately 1.5 cm. (b) In order to reduce the Q and improve AR, some transducers have an absorber added on the rear face of the transducer.

this might be accomplished. Instead of air on the back side of the transducer, a material having an acoustic impedance much closer to the transducer's impedance is placed in close contact with the rear transducer face. This allows power to flow out the rear of the transducer in addition to that radiated into the tissue, thus lowering the transducer's Q. If the backing material is a good ultrasound absorber, this power is permanently lost. Absorber materials that have been successfully used include aluminum-filled epoxy and tungsten-filled epoxy. Problem 5.8 shows that an absorber-

backed transducer will possess a lower Q and better AR than an air-backed one.

Equation (5.25) also reveals an important relationship between resolution and wavelength. The shorter the wavelength, the better will be the instrument's ability to resolve detail since a small value for axial resolution leads to improved measurement of spacings. For good resolution, an ultrasonic instrument should employ as high a frequency (as short a wavelength) as possible, limited only by the increased attenuation at the higher frequencies. For example, adult echocardiography is normally done at 2.25 MHz as a compromise between resolution and penetration. Pediatric echocardiography, however, will use frequencies as high as 5 MHz to improve resolution, since the path length into the heart is shorter in children and higher attenuation per centimeter is therefore allowed.

There are several practical factors that cause the actual axial resolution of a typical medical instrument to be worse than predicted by Equation (5.25). One is due to the frequency dependence of tissue absorption, called dispersive absorption, which will effectively lengthen the pulse as it travels through intervening tissue. As discussed in Chapter 4, most tissues show a linear increase in absorption with increasing frequency; high frequencies are attenuated much more than lower frequencies. A sharp pulse of transmitted acoustical energy (such as shown in Figure 5.7) actually contains a wide spectrum of frequency components, obtained by Fourier analysis of the time waveform of the pulse. The sharper the pulse, the higher the frequencies contained in its spectrum. (It can be said that the high-frequency components contribute to the "sharpness" of the pulse.) When this pulse travels through tissue, these higher frequencies are selectively lost at a faster rate than the low-frequency components are. The result is a stretching of the pulse time leading to worse axial resolution between neighboring reflectors.

Another factor is any electronic compression which may be purposely added in the receiver stages of the instrument to decrease its signal dynamic range before the display (covered in Chapter 6). Often, logarithmic compression is employed. Compression has the effect of minimizing the differences between large-amplitude signals and small-amplitude signals. When applied to the pulse waveform shown in Figure 5.7, it can be seen that the effect is to boost the tail of the pulse and therefore to effectively lengthen the pulse in time as seen on the display, again leading to a worsening of the axial resolution.

5.3 BEAM PATTERNS

We now turn our attention to the description of the shape of the radiating beam from the transducer. The behavior of this beam is important in

determining the spatial sensitivity of the imaging instrument, both in the transmit and the receive modes.

The pressure wave that propagates from the face of an unfocused transducer generally maintains the approximate lateral dimensions of the transducer for a certain distance, but natural divergence begins to spread the transverse extent of the beam at larger distances so that the beam takes on a diverging nature. In the region near the transducer (the "near field"), the beam has many amplitude and phase irregularities due to interference between the contributing waves from all parts of the transducer's face, whereas in the region further from the transducer (the "far field"), the beam profile is much more uniform and well behaved. To quantitatively define the transition distance between these near-field and far-field regions, and to more precisely determine the amount of beam spreading in the far field, we next mathematically solve for the radiation pattern from an ultrasonic transducer.

The geometry of the problem is given in Figure 5.11; a circular coordinate system is initially assumed. The coordinates of the source points in the plane of the transducer face are denoted ρ and θ, and the coordinates pointing to the observation point where the pattern is sought are denoted r and ϕ. The distance from the source points to the observation point is given by r'. For circularly symmetric situations no generality is lost by letting the observation points lie on the x_1 axis. From geometry (see Problem 5.11),

$$r' = (r^2 + \rho^2 - 2r\rho \cos\theta \sin\phi)^{1/2} \tag{5.26}$$

To analyze the observed radiation pattern, we rely upon Huygen's principle, which states that the radiation pattern from a general extended source can be constructed by considering the source as an appropriately weighted collection of point sources, each radiating outwardly propagating spherical waves. To get the complete radiation pattern, the contributions

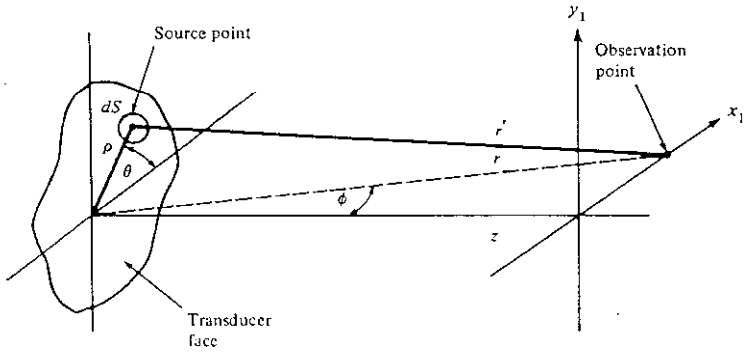

Figure 5.11 The general coordinates for solving for the radiation pattern from an ultrasound transducer.

of all spherical waves from all point sources comprising the transducer are added (magnitude and phase) at the point of observation. This decomposition of the complex problem into a summation of simpler parts (i.e., spherical waves radiating from point sources) is allowed because the wave equation is a linear equation in the pressure variable, as shown in Problem 2.7.

Each point on the transducer face, then, is assumed to be the radiator of a spherical pressure wave, the form of which is

$$dp = \frac{kZu_0}{2\pi r'} \cos\left(\omega t - kr' + \frac{\pi}{2}\right) dS \tag{5.27}$$

where dp is the incremental pressure contribution at the observation point due to a spherical wave from a point source of incremental size dS, k is the propagation constant of the wave ($k = 2\pi/\lambda$), Z is the acoustical impedance of the intervening medium, and r' is the distance from source to observation point as given by Equation (5.26). Note that the pressure decreases as a function of $1/r'$ away from the point source; this is consistent with the $1/r^2$ dependence of power density expected from the conservation of energy principle applied to a diverging spherical wave. In obtaining Equation (5.27), the transducer face was assumed to be vibrating with a sinusoidal velocity of $u = u_0 \cos(\omega t)$ perpendicular to the ρ–θ plane.

The total pressure at the observation point is the integral of the incremental pressures:

$$p = \int_{\text{source}} dp \tag{5.28}$$

Assuming all portions of transducer face are oscillating with the same velocity and are in phase with each other, as would be the case for a rigid, pistonlike transducer, Equations (5.27) and (5.28) may be combined to give

$$p = \frac{kZu_0}{2\pi} \int_{\text{source}} \frac{\cos(\omega t - kr' + \pi/2)}{r'} \rho \, d\rho \, d\theta \tag{5.29}$$

where $\rho \, d\rho \, d\theta$ has been substituted for dS. For a general transducer shape and for an arbitrary observation point, this equation is quite difficult to evaluate and usually requires a computer solution. But it may be evaluated for some simple cases, as shown below.

5.3.1 Near-Field Pattern (On-Axis) of a Circular Transducer

Consider the transducer to be a circular disc of radius a. In the near-field region, r' is not large enough to allow a mathematical simplification of its form, so Equation (5.29) is still too complex for a general solution.

We therefore restrict our observation points to be on the z axis, such that $\sin\phi = 0$ and $r = z$. Equation (5.26) then reduces to

$$r' = \sqrt{\rho^2 + z^2}$$

Figure 5.12 shows the geometry for this special case. Substituting for r' in Equation (5.29) gives

$$p(z,t) = \frac{kZu_0}{2\pi}\int_0^a \frac{\cos(\omega t - k\sqrt{\rho^2+z^2} + \pi/2)}{\sqrt{\rho^2+z^2}}\rho\, d\rho \int_0^{2\pi} d\theta$$

Changing variables to $\beta = \sqrt{\rho^2+z^2}$ and using straightforward integration leads to

$$\begin{aligned} p(z,t) &= -Zu_0[\sin(\omega t - k\sqrt{a^2+z^2} + \pi/2) - \sin(\omega t - kz + \pi/2)] \\ &= Zu_0[\cos(\omega t - kz) - \cos(\omega t - k\sqrt{a^2+z^2})] \end{aligned} \tag{5.30}$$

This result for the on-axis pressure amplitude has a very interesting interpretation. Note that the first term in the equation, $Zu_0\cos(\omega t - kz)$, is just the familiar form for a pressure wave that appears to be coming from the center of the transducer, whereas the second term, $Zu_0\cos(\omega t - k\sqrt{a^2+z^2})$, which subtracts from the first, appears to be a wave coming from a point at the edge (radius = a) of the transducer. The combination of these two waves, with phases that change at different rates as z varies, provides the destructive and constructive interference pattern which produces the irregularities found in the near field.

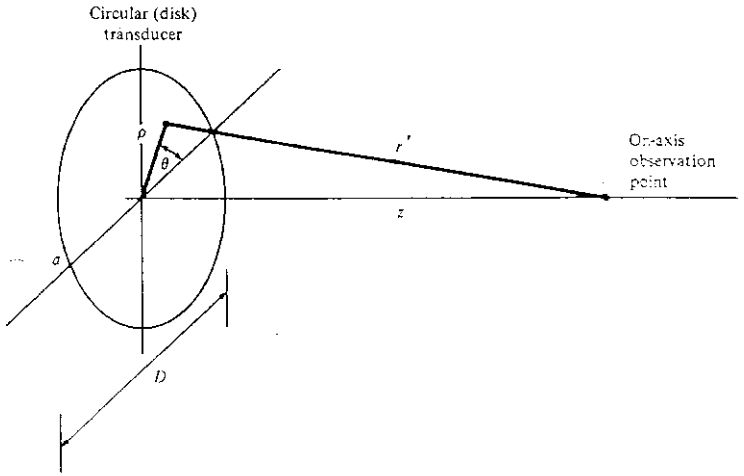

Figure 5.12 Geometry for calculating the near-field on-axis pressure field from a circular transducer of radius a and diameter D.

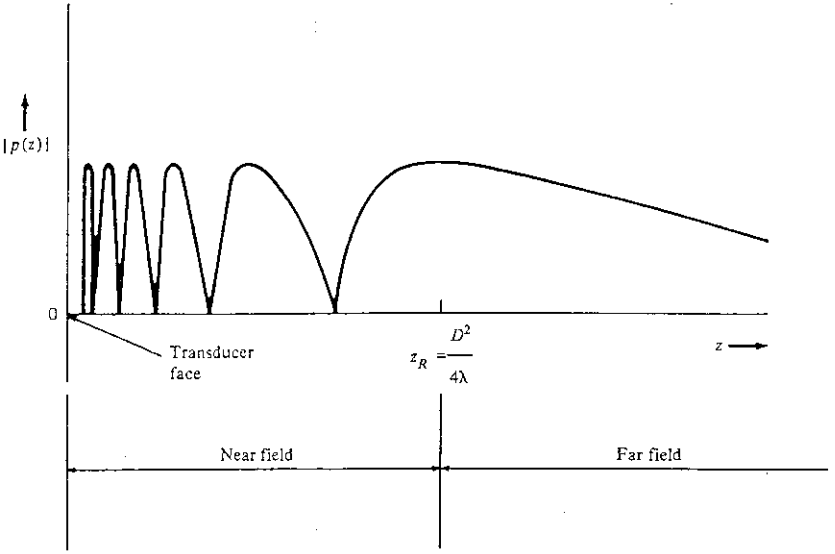

Figure 5.13 Variation of the magnitude of on-axis pressure field from a circular transducer of diameter D. This is a plot of the absolute magnitude of Equation (5.30) at one particular time, $t = 0$, and is the envelope of the oscillating pressure. The transition point from the near field to the far field is defined as the position of the furthest maximum. Beyond that point the field is more uniform.

A plot of the magnitude of Equation (5.30), shown in Figure 5.13, reveals the rapid variation of on-axis pressure in the near field of a circular transducer. Note that there is a multitude of points in the near field where the pressure actually goes to zero (complete destructive interference) and that the rapidity of the spatial oscillation of the pattern decreases as one moves further away from the face of the transducer. In fact, at large distances from the face of the transducer, the resultant pressure amplitude is no longer oscillatory but behaves as a slowly decreasing ($1/z$) field; this is the far field.

To mark the transition from near-field to far-field behavior, it is reasonable to choose the on-axis point where Equation (5.30) has its last maximum for increasing z. This is the value of z for which the phase difference between the first cosine term and the second cosine term in Equation (5.30) is just equal to π, so both terms are positive and the two terms add. Thus, if the transition point is denoted z_R, then

$$k\sqrt{a^2+z_R^2} - kz_R = \pi \tag{5.31}$$

Since $z_R \gg a$ for a transducer many wavelengths in radius, the radical in Equation (5.31) may be approximated as

$$\sqrt{a^2 + z_R^2} \approx z_R + \frac{a^2}{2z_R}$$

Then Equation (5.31) becomes

$$kz_R + \frac{ka^2}{2z_R} - kz_R = \pi$$

Rearranging yields

$$\boxed{z_R = \frac{a^2}{\lambda} = \frac{D^2}{4\lambda}} \tag{5.32}$$

For many unfocused transducers used in medical imaging, the body structures being imaged are not wholly in the far field of the radiation pattern where the fields are desirably uniform. For a 2-cm-diameter transducer at 2.25 MHz, the transition distance is z_R = 15 cm, rather deep.

If the transducer face is square or rectangular rather than round, the above equations do not strictly apply. For example, the pressure in the near field never goes exactly to zero anywhere as it does for a circular transducer. Nonetheless, the pressure magnitude has many peaks and valleys in the near field, and the qualitative description of the irregular near-field behavior making a transition to a more uniform far-field behavior is still valid. This is shown in Figure 5.14, where intensity maps (proportional to the square of pressure) are given at three progressively farther distances from a square transducer. The smoothing of the beam irregularities at greater distances is evident; however, even the most distant map shown in the figure is not yet in the far field of the transducer.

5.3.2 Far-Field Pattern of an Ultrasound Transducer

When the beam is observed at a large distance from the transducer, simplifications can be made in the general Equation (5.29) that allow the field to be calculated at any point (off-axis as well as on-axis) in the plane of observation. The approximations appear at two places in Equation (5.29). First, in the far field the magnitude of the r' term which appears alone in the denominator of the integrand will not differ appreciably from r over the range of the source integration, since r is much greater than the source dimensions. This r' is therefore set equal to r (a constant with respect to the integration variables) and is brought out of the integral.

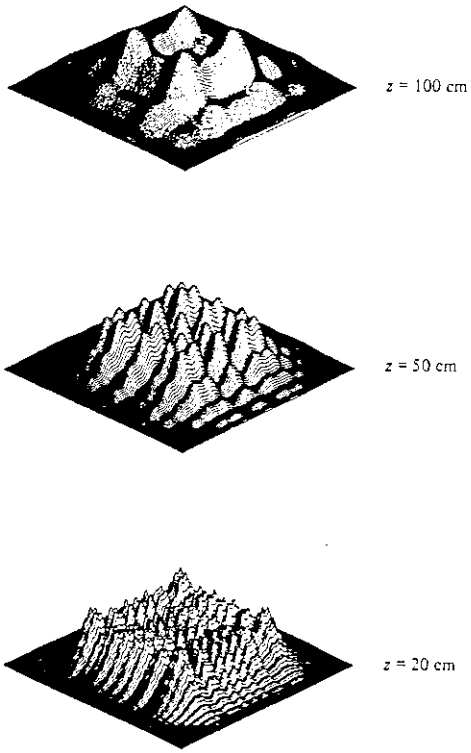

Figure 5.14 Radiation intensity maps at three planes progressively more distant from a square transducer face. Note the progression toward a more uniform distribution. The transducer is 5 cm × 5 cm operating at 3 MHz. Data from P. C. Pedersen and D. A. Christensen, *Acoustical Holography* 6 (1975), 711–739, Plenum Press.

Second, the r' term in the argument of the cosine also may be approximated, but since this r' is multiplied by k $(= 2\pi/\lambda)$, and since λ is small at ultrasonic frequencies (making k large), this approximation cannot be as rough as letting $r' = r$ = constant; the phase term kr' may vary several radians over the source integration, causing several oscillations of the cosine term. To preserve this interference effect in the integration, only a partial simplification of r' from Equation (5.26) is made, known as the Fraunhofer approximation. If the observation distance is far enough away from the

source that the source appears small compared to the observation length, then $r \gg \rho$ and Equation (5.26) may be approximated by

$$r' \approx r - \rho \cos\theta \sin\phi \tag{5.33}$$

Putting Equation (5.33) into the phase term of Equation (5.29) and letting $r' = r$ in the denominator as discussed above gives

$$p(\phi, r, t) = \frac{kZu_0}{2\pi r}\int_{\text{source}} \cos\left[\omega t - kr + k\rho\cos\theta\sin\phi + \frac{\pi}{2}\right]\rho\, d\rho\, d\theta$$
$$= K\int_{\text{source}} \cos[\Psi(t) + k\rho\sin\phi\cos\theta]\rho\, d\rho\, d\theta \tag{5.34}$$

where

$$K = \frac{kZu_0}{2\pi r}$$

and

$$\Psi(t) = \left(\omega t - kr + \frac{\pi}{2}\right)$$

K and $\Psi(t)$ are constants with respect to integration over the source coordinates ρ and θ. The result of this integration will depend upon the particular shape of the transducer. Two cases are considered next.

Circular Disk Transducer of Radius a

For a circularly symmetric source, the limits of integration become simply

$$p(\phi, r, t) = K\int_0^a\int_0^{2\pi} \cos[\Psi(t) + k\rho\sin\phi\cos\theta]d\theta\ \rho\, d\rho$$

Using the trigonometric identity $\cos(A + B) = \cos A\cos B - \sin A\sin B$ gives

$$p(\phi, r, t) = K\int_0^a\left[\cos\Psi(t)\int_0^{2\pi}\cos(k\rho\sin\phi\cos\theta)d\theta - \sin\Psi(t)\int_0^{2\pi}\sin(k\rho\sin\phi\cos\theta)d\theta\right]\rho\, d\rho \tag{5.35}$$

The last integral in this equation is zero since the sine term is an odd function of the cyclical argument ($\cos\theta$) as θ ranges from 0 to 2π. The other integral over θ is of the form which results in a Bessel function, as given in reference texts on Bessel functions:

$$\int_0^{2\pi}\cos(x\cos\theta)d\theta = 2\pi J_0(x)$$

where J_0 is the Bessel function of the first kind with order zero. Therefore, Equation (5.35) becomes

$$p(\phi, r, t) = 2\pi K\cos\Psi(t)\int_0^a J_0(k\rho\sin\phi)\rho\, d\rho \tag{5.36}$$

This integral, in turn, can be evaluated by the relation

$$\int xJ_0(x)dx = xJ_1(x)$$

where J_1 is the Bessel function of the first kind with order 1. Then, Equation (5.36) becomes (see Problem 5.13)

$$p(\phi, r, t) = \pi a^2 K\cos\Psi(t)\left[\frac{2J_1(ka\sin\phi)}{ka\sin\phi}\right] \tag{5.37}$$

The instantaneous radiated power density pattern may be found from $I = p^2/Z$, and reinserting the previous definitions for K and $\Psi(t)$ yields

$$I(\phi, r, t) = \frac{\pi^2 a^4 u_0^2 Z\sin^2(\omega t - kr)}{\lambda^2 r^2}\left[\frac{2J_1(ka\sin\phi)}{ka\sin\phi}\right]^2 \tag{5.38}$$

Some interesting observations about the far-field radiation pattern from a circular transducer may be obtained from Equation (5.38). First, note that the power density decreases as $1/r^2$ in this region, as would be expected when the measurements are made far enough away that the source appears as a small radiator of diverging waves. More importantly, the distribution with respect to angle behaves according to the term in the square brackets, the so-called directional factor:

$$H_c(\phi) = \left[\frac{2J_1(ka\sin\phi)}{ka\sin\phi}\right] \tag{5.39}$$

To obtain a feeling of the shape of this far-field pattern, it may be plotted on an observation screen a distance z away from the transducer. If the angles of divergence of the beam are not too great, the small angle approximation

$$\sin\phi \approx \frac{x_1}{z} \tag{5.40}$$

may be used, where x_1 is the coordinate in the plane of observation; refer to Figure 5.11. Then, the directional factor Equation (5.39) may be written in terms of distance on the observation plane:

$$H_c(x_1) = \left[\frac{2J_1(kax_1/z)}{kax_1/z}\right] \tag{5.41}$$

The square of this term is plotted in Figure 5.15a and gives an indication of the extent of the power density pattern at a distance z from the transducer. Due to the denominator of $H_c(x_1)$ and the behavior of J_1, the power density drops off rapidly as x_1 increases from the center of the pattern. Also, there are repetitive zeros and side peaks as the Bessel function J_1 oscillates with the increasing arguments.

The great majority of power is contained in the central (main) lobe of the pattern between the first zeros on either side of this central peak. However, some power is found in the side lobes which neighbor the main lobe. The extent of the main lobe may be defined as occupying the area between the first zeros; these zeros occur at

$$J_1(\pm 3.83) = 0 \tag{5.42}$$

or

$$x_1 = \pm 3.83 \frac{z}{ka}$$

as shown in Figure 5.15a. Note that the width of the main lobe increases linearly with distance z in the far-field region.

Returning now to the angular dependence of the far-field radiation pattern, Equation (5.39) shows that the pattern may be considered to be a circularly symmetric function of the angle ϕ via the term sin ϕ; this equation is valid even for large ϕ. An angular plot of the logarithm of the square of Equation (5.39) in terms of decibels (to compress the range) is given in Figure 5.15b in polar coordinates; such a plot is sometimes referred to as the *antenna* pattern of the radiator. To obtain such a specific angular plot, a value of the transducer radius a must be given. For this figure, the transducer diameter is assumed to be 10 wavelengths wide, so $a = 5\lambda$ or $ka = 10\pi$.

The angular position of the first zero defines the amount of divergence (half-angle) ϕ_d of the main lobe as it propagates from the source; from Equation (5.42),

$$\sin \phi_d = \frac{3.83}{ka}$$

or

$$\boxed{\phi_d = \sin^{-1}\left(0.61 \frac{\lambda}{a}\right)} \tag{5.43}$$

It is convenient to use this angle as a measure of divergence of the beam from a circular transducer, although some authors consider it too conservative. The smaller angular width to the half-power points (−3 dB) rather than to the zeros is sometimes used; twice this angle is known as the Full Width to Half Maximum (FWHM) of power density. In this text, however, we shall use ϕ_d given by Equation (5.43) as the measure of divergence (half-angle) for reasons that will become clear when the concept of lateral resolution is discussed.

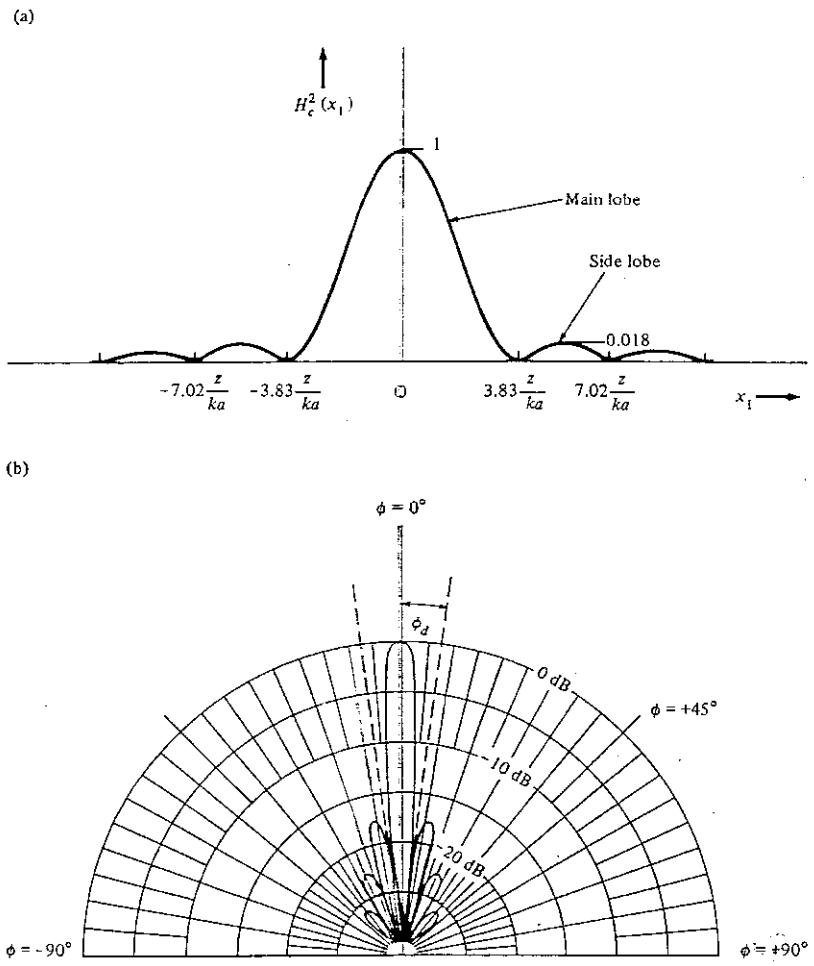

Figure 5.15 (a) The far-field power density pattern observed at a distance z from a circular transducer of radius a. (b) An angular plot of the same pattern in polar coordinates. The intensity is plotted in logarithmic (decibel) units. In this example, the transducer diameter equals 10 wavelengths.

Note the inverse relationship in Equation (5.43) between ϕ_d and the transducer radius a. When a is a large number of wavelengths (as measured in the tissue), the far-field beam is highly directed; conversely, when a is small, the beam spreads considerably as it propagates from the transducer. In fact, when a is approximately one-half a wavelength (i.e., the diameter is one wavelength) or smaller, the half-angle of divergence is greater than 90° and the beam appears to be radiating hemispherically more or less isotropically from a point source.

A word of caution regarding the use of far-field patterns: Most single transducers used in medical imaging are many tissue wavelengths in diameter so the transition distance z_R is large enough for the reflecting objects to fall in the near-field region. Also, the transducers are often *focused* by an integral lens (covered in Section 5.5). In either case, the far-field divergence angle ϕ_d does not directly apply to the imaged region. However, multiple-element transducers, such as the linear arrays found in real-time scanners and discussed at the end of this chapter, are usually made of a series of small unfocused elements, and the radiation pattern from each of these small elements *is* determined by the far-field considerations of Equation (5.43). Also, for focused transducers the shapes of the beams in the focal plane will be shown later to be scaled-down versions of the far-field patterns found above.

Rectangular Transducer of Dimensions b × h

The analysis of the far-field radiation from a rectangularly shaped transducer with width b in the x_0 direction and height h in the y_0 direction proceeds from Equation (5.34) in a manner similar to that outlined above for a circular one; Figure 5.16a shows the orientation. Note that in the source plane, $\rho \cos\theta = x_0$. Initially restricting our observation to be along the x_1 axis ($\phi = \phi_x$), Equation (5.34) may be integrated over the rectangular source to give (see Problem 5.14)

$$p(\phi_x, r, t) = bhK \cos \Psi(t) \left[\frac{\sin[(kb \sin \phi_x)/2]}{(kb \sin \phi_x)/2} \right] \tag{5.44}$$

A similar expression holds for observations along the y_1 axis ($\phi = \phi_y$), and since the source is the shape of a rectangle whose boundaries may be expressed by equations that are mathematically separable in x_0 and y_0, the complete expression for far-field power density from a rectangular transducer is also separable in ϕ_x and ϕ_y:

$$I(\phi_x, \phi_y, r, t) = \frac{b^2 h^2 u_0^2 Z \sin^2(\omega t - kr)}{\lambda^2 r^2} \left[\frac{\sin[(kb \sin \phi_x)/2]}{(kb \sin \phi_x)/2} \frac{\sin[(kh \sin \phi_y)/2]}{(kh \sin \phi_y)/2} \right]^2$$

(a)

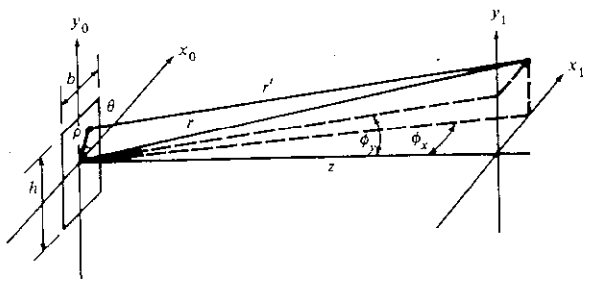

(b)

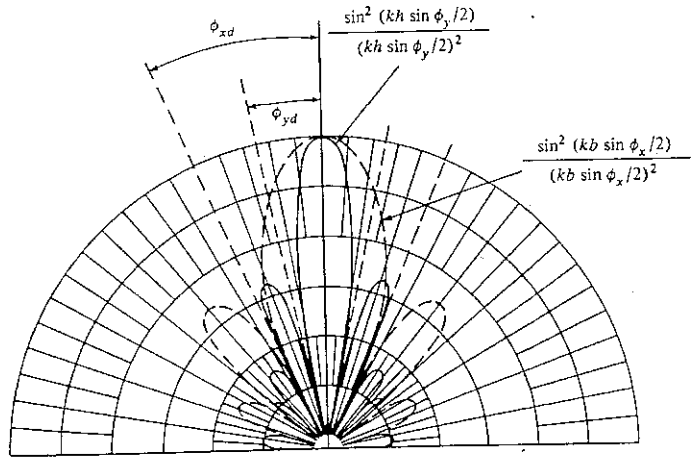

Figure 5.16 (a) The geometry for determining the far-field radiation from a rectangular transducer. (b) The far-field power density pattern as observed in the x_1 direction superimposed on the pattern in the y_1 direction.

The term in the square brackets is the directional factor:

$$H_r(\phi_x, \phi_y) = \left[\frac{\sin[(kb \sin \phi_x)/2]}{(kb \sin \phi_x)/2} \frac{\sin[(kh \sin \phi_y)/2]}{(kh \sin \phi_y)/2} \right] \tag{5.45}$$

The far-field beam pattern from a rectangular element has the same qualitative features as those described for a circular source, such as main lobe, side lobes, and so on, except that the directionality now has the form

(sin x)/x. Note that the half-angle to the first zero marking the extent of the main lobe is now given in the x_1 direction by

$$\sin\left(\frac{kb \sin \phi_{xd}}{2}\right) = 0$$

or

$$kb \sin \phi_{xd} = 2\pi$$

or

$$\boxed{\phi_{xd} = \sin^{-1}\left(\frac{2\pi}{kb}\right) = \sin^{-1}\left(\frac{\lambda}{b}\right)} \tag{5.46}$$

A similar equation describes the divergence as measured in the y_1 direction:

$$\boxed{\phi_{yd} = \sin^{-1}\left(\frac{\lambda}{h}\right)} \tag{5.47}$$

Figure 5.16b shows that, as opposed to the pattern from a circular transducer, the pattern here is asymmetric. The inverse relationship between size and divergence angle still applies, however. For a rectangular element that is taller than it is wide (i.e., $h > b$), the far-field radiation pattern of the element will be wider than it is tall [i.e., $\phi_{xd} > \phi_{yd}$ from Equations (5.46) and (5.47)]. More will be said about rectangular radiation patterns when arrays of small elements are discussed at the end of this chapter.

5.4 WIDTH OF BEAM IN NEAR FIELD AND FAR FIELD

As the previous section described, the beam pattern in the near field has a very irregular interior, with many peaks and valleys, especially near the transducer face; Figure 5.14 showed this. The lateral extent of the near field is roughly confined to the size of the transducer, although it must be admitted that it is difficult to precisely define the edge of such an irregular field.

As the beam progresses into the far field, its topology becomes much more smooth, eventually evolving into a well-defined single main lobe with low-intensity side lobes as shown in Figure 5.15a. The edges of this beam now spread linearly with distance, and the width of the main lobe, as given by the half-angle ϕ_d to the first zero on each side, asymptotically diverges at a constant angle inversely proportional to the transducer diameter and therefore the near-field beam diameter.

This progressive spreading of the beam width is diagrammed qualitatively in Figure 5.17. In the near field, also known as the Fresnel region, the beam is nearly collimated until it approaches the transition distance z_R. At this point the beam has started to spread a little. (Some authors define a "transition zone" here between the near field and the far field within which the beam changes its character from nearly collimated edges to diverging edges.)

As it travels into the far field, also known as the Fraunhofer region, the beam widens further and eventually approaches the constant angle of

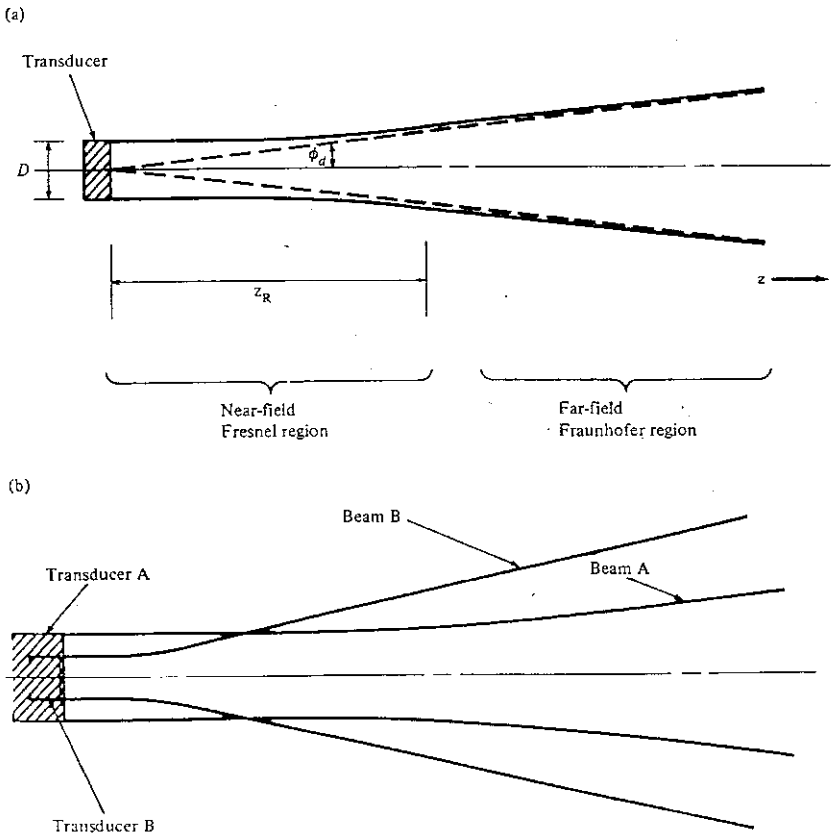

Figure 5.17 (a) The shape of a beam as it propagates away from an unfocused transducer. The beam stays approximately collimated in the near field, but diverges linearly in the far field approaching a half-angle ϕ_d. (b) The beam from a small transducer diverges more rapidly than the beam from a larger transducer.

divergence ϕ_d. It is interesting to note in Figure 5.17b that the beam from a small transducer (transducer B) starts small but eventually becomes larger since it possesses a shorter z_R and greater ϕ_d than transducer A.

Smoothing the Beam's Profile

The irregularities within the near field and the presence of side lobes in the far field are sometimes an inconvenience when attempting to predict the returns from reflectors in the beam's pattern. There is a technique for smoothing out these irregularities, although a price is paid. It is based upon the fact that, if the beam's amplitude profile as a function of radius was Gaussian-shaped at the transducer face (peaked at the center and decreasing to zero as $\exp(-\rho^2/a_1^2)$ toward the edges) rather than being the uniform amplitude across the transducer face assumed above, then the radiated beam's profile would be smoothly Gaussian-shaped *everywhere* in the near field as well as in the far field.

Therefore, if by some means the transducer excitation profile approximates a Gaussian form with decreasing activity away from the center, the beam would be expected to be more uniform in its transverse behavior. Various ways of achieving a shaded profile at the radiating surface include placing a radially varying absorber in front of the transducer, designing the transducer face to have a star shape with some unexcited areas near the edges, or by using a concentric ring transducer ("bull's-eye") and exciting the outer rings with progressively less drive voltage than the center rings. All these techniques, known as *apodization* because they reduce the "feet" (side lobes) in the radiated beam pattern, will produce an overall smoother beam profile. The disadvantages, however, are that less total power is radiated, the transducer is more complex, and, as Equation (5.43) shows, the beam diverges at a greater angle since the effective transducer diameter is smaller.

5.5 FOCUSING WITH LENSES, AND LATERAL RESOLUTION

The beam width from an unfocused transducer is generally too wide to give adequate definition of the fine lateral features of objects being imaged. Therefore, a lens or other focusing scheme such as a spherical reflector is usually employed to converge the radiating beam into a spot at the focal plane of the lens. However, the size of the focused beam cannot be infinitely small, since the natural divergence of a propagating wave as described in

the previous section will attempt to spread even a converging beam, reducing the focusing effect of the lens. The further away the focal plane is from the lens, the larger the focused spot will be.

The equations of Section 5.3 can be used to evaluate the size of the focused spot once they are modified to include the effects of the lens. As in optics, an acoustical lens is fabricated from a disk of material by forming a curved refracting surface on one or both of its faces; Figure 5.18 shows the cross-section of a plano-concave focusing lens. As opposed to optics,

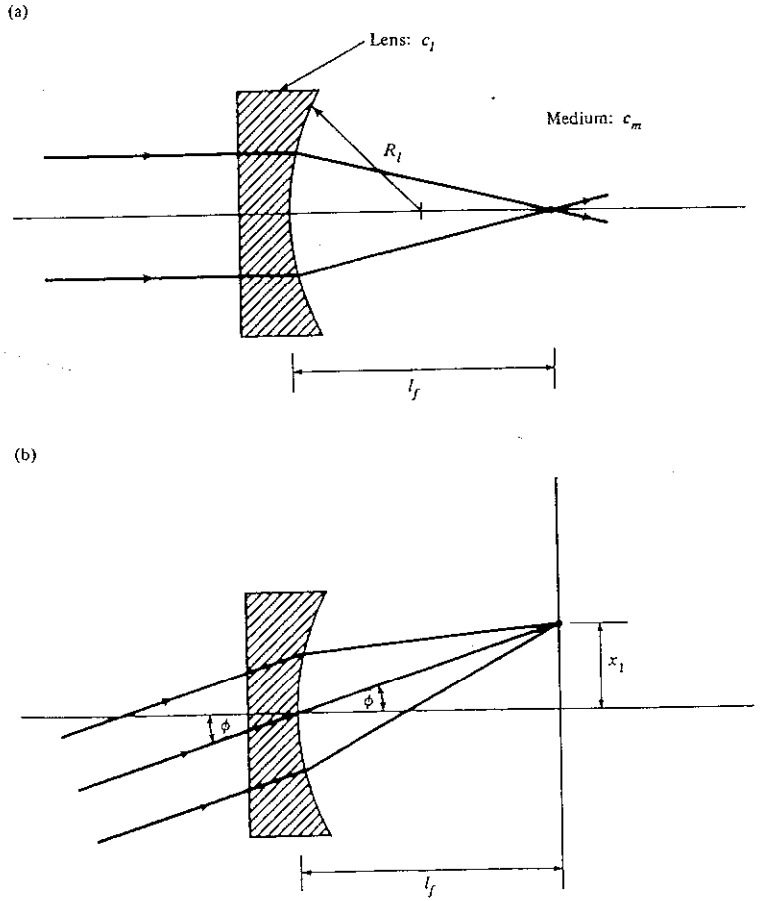

Figure 5.18 (a) A focusing lens made of material (such as polystyrene) with phase velocity greater than in the surrounding medium. (b) A lens has the property of transforming angles into position on the focal plane.

the lens material generally possesses an acoustic phase velocity which is *greater* than that of the material surrounding it (water or tissue). Thus, a converging (positive) lens will have a concave face. Problem 5.18 uses Snell's law for ray tracing to show that a plano-concave lens having a surface with radius of curvature R_l will produce focusing at a focal length equal to

$$l_f = \frac{R_l}{1 - \frac{c_m}{c_l}} \tag{5.48}$$

where c_l is the phase velocity of the lens material and c_m is the phase velocity of the medium into which the wave is focused.

Lenses have the property of transforming angles into position. That is, all rays entering the lens at a common angle ϕ will get directed to a radius x_1 on the focal plane as shown in Figure 5.18b. Under the small-angle approximation, geometry gives the transformation relationship as

$$\sin\phi \approx \frac{x_1}{l_f} \tag{5.49}$$

Therefore, a lens of focal length l_f placed in front of the beam from a circular transducer whose radiation pattern is given by Equation (5.39) will transform the far-field angular distribution into a spatial distribution on the focal plane via the transformation of Equation (5.49). Making this substitution into Equation (5.39) yields the spatial distribution of the pressure at a focused spot from a circular transducer of radius a:

$$H_c(x_1) = \left[\frac{2J_1(kax_1/l_f)}{kax_1/l_f}\right] \tag{5.50}$$

and the *focused* pattern looks exactly like the far-field pattern of Figure 5.15a, except that it is scaled down by an amount l_f/z. Figure 5.19 shows how the focused spot would appear face-on.

Size of Focused Spot

The focused spot has a dense central portion (corresponding to the main lobe) surrounded by minor rings (the side lobes). The diameter of the central portion is defined as previously: the distance between the first zeros bounding the main lobe. From Equation (5.50) the radius of the first zero is found at

$$x_1 = \frac{3.83 l_f}{ka} = \frac{0.61 l_f \lambda}{a}$$

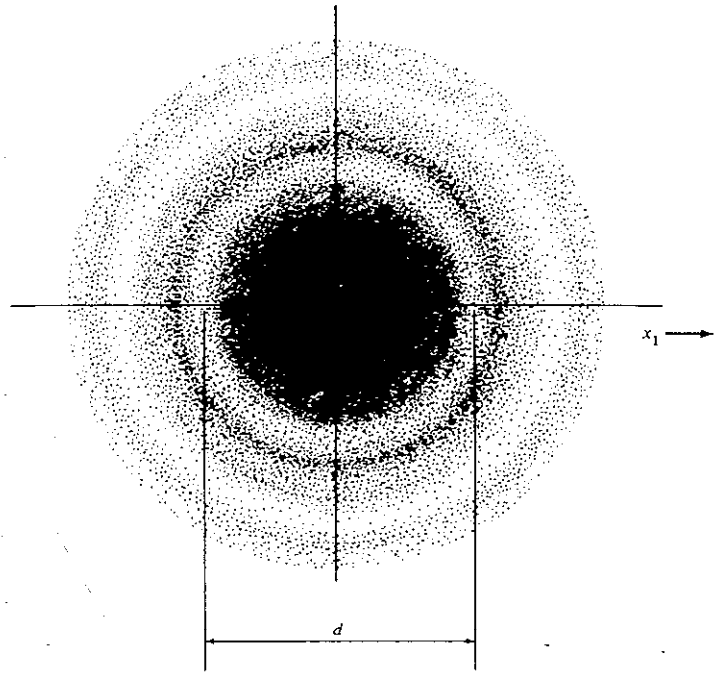

Figure 5.19 The greatly magnified pattern of a focused spot from a lens of focal length l_f. The entering beam diameter is D.

or, put in terms of original beam (transducer) diameter $D = 2a$, the diameter between first zeros is the focused spot diameter $d = 2x_1$:

$$\boxed{d = 2.44\left(\frac{l_f}{D}\right)\lambda} \tag{5.51}$$

Figure 5.20 defines the quantities entering Equation (5.51).

For the case of a rectangular transducer of width b, an analogous development can be undertaken to find the width w of the focused spot in the direction parallel to b. Using Equations (5.44) and (5.49), the result for a rectangular transducer is

$$\boxed{w = 2\left(\frac{l_f}{b}\right)\lambda} \tag{5.52}$$

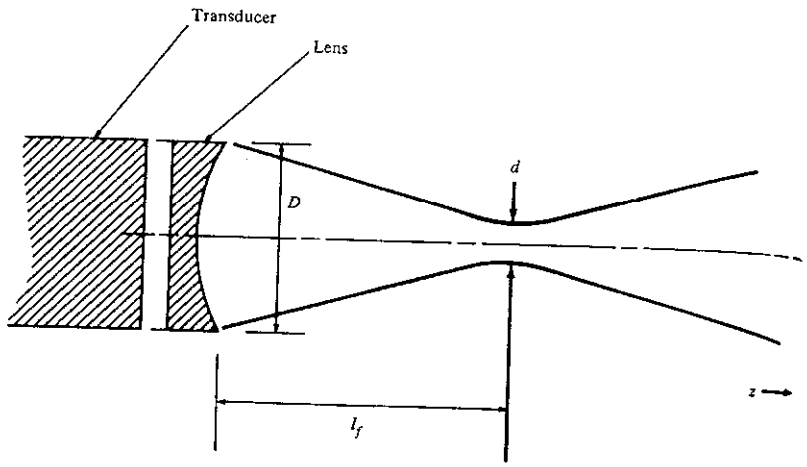

Figure 5.20 A lens will focus the beam to a small spot, but the size d of the focused spot depends upon l_f, D, and λ according to Equation (5.51).

The effects of divergence are manifested in these relationships. In Equation (5.51) the larger the diameter D of the transducer, the smaller is the tendency of divergence to expand the beam, and the smaller the spot of focus. Also, the further away the position of focus l_f, the greater is the effect of divergence, leading to a larger d.

How small can the beam be focused practically? The ratio in the parentheses in Equation (5.51) is known as the "f-number" of the lens; and due to practical limitations such as spherical aberration, it is difficult to fabricate a quality lens whose f-number is much smaller than unity. Therefore, as a rule of thumb, it can be said that the smallest possible focused spot is on the order of the wavelength of radiation used.*

Not only is it impossible to focus to an infinitely small spot, it may be impossible to get any narrowing at all in the beam diameter if the attempted focal distance is too far away. Equation (5.51) shows that d will be greater than D if

$$l_f > \frac{D^2}{2.44\lambda} \approx z_R \tag{5.53}$$

or, in other words, no focusing occurs if the focal length of the lens is greater than about the transition distance. Thus, it may be said that focusing is only possible at distances within the near field, not in the far field of a transducer.

* This limitation appears in optics and general quantum-mechanical wave analyses as well as in acoustics.

Lateral Resolution

The spot size of the focused beam determines the transverse spatial resolution of a medical ultrasound imager, as indicated in Figure 5.21. Here, the focused beam is swept uniformly past a pair of point reflectors. The waveform of the envelope of the received echoes depends upon the lateral spacing of the points. When far apart, the echoes from each point are distinct, and it is clear that there are two separate points. As they move closer, however, approaching the spacing d, the separate echoes start to blend together, and at some stage the points are so close that their echoes cannot be separately resolved: that is, they appear as one reflecting object.

The spacing in the transverse plane at which the points are just separately resolvable is known as the *lateral resolution* (LR); and from Figure 5.21 a reasonable measure of LR is the diameter of the focused spot d. That is,

$$LR \approx d$$

and the motivation for focusing the beam to reduce the focused spot size d in an imaging system is obvious. Using Eq. (5.51) for a circular transducer,

$$\boxed{LR \approx 2.44\left(\frac{l_f}{D}\right)\lambda} \tag{5.54}$$

This relationship, along with the previous expression for axial resolution, is restated in Table 5.2.

We can now make an important observation: The resolution in all directions (axial and lateral) is closely related to wavelength, and as a practical matter cannot be made smaller than the wavelength used. Therefore, high resolution machines will employ as high a frequency as possible, until increasing attenuation takes the signal to the lower limit of the signal-to-noise ratio. Echo instruments for imaging tiny objects in the eye, for instance, may go as high as 15 MHz since the absorbing path length is so short there.

Depth of Focus

There is one disadvantage to tight focusing of the beam. Although it improves lateral resolution for reflecting objects located in the plane of focus, points in planes either nearer or further away than the focal length are compromised because the beam is somewhat larger than d on either side of the focal plane. The problem gets worse with decrease in the focused size, as shown in Figure 5.22.

The axial distance over which the beam maintains its approximate focused size is termed the depth of focus. To obtain an estimate of this

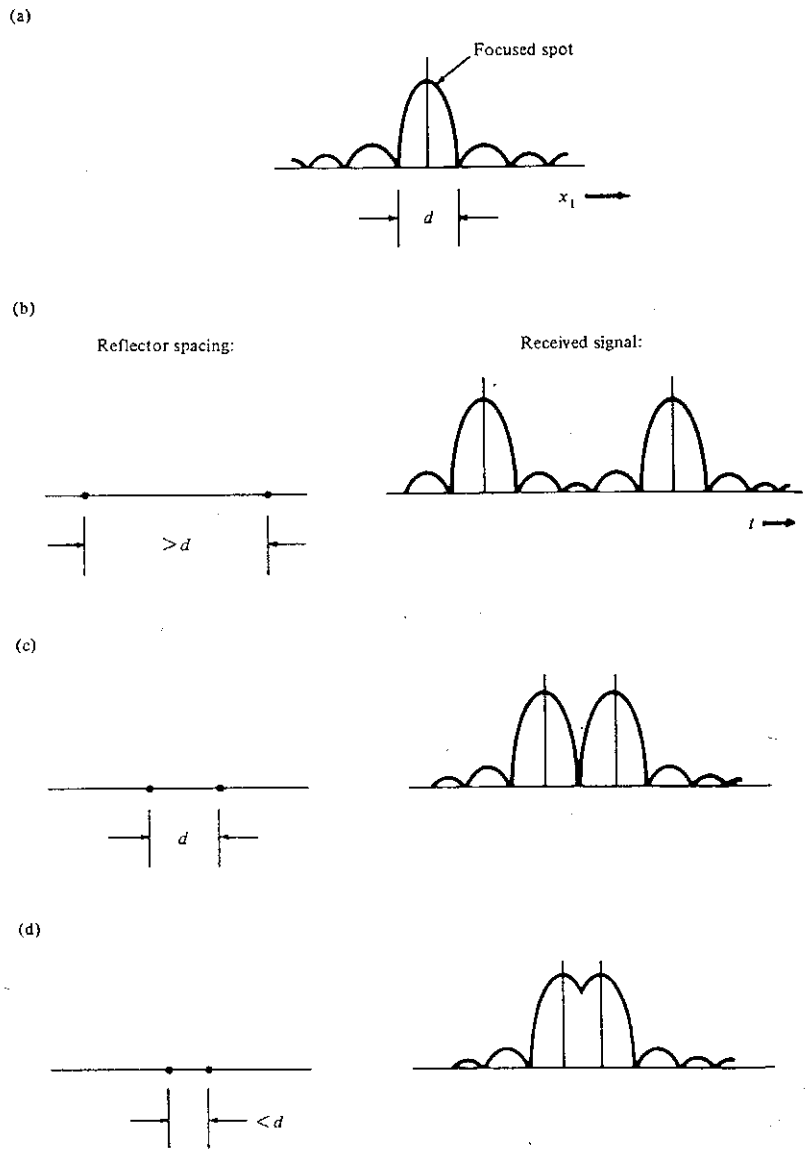

Figure 5.21 (a) The lateral spatial resolution is determined by the size d of the focused spot. (b)–(d) The signal received from a pair of point reflectors as their lateral spacing is progressively narrowed.

TABLE 5.2 THEORETICAL EXPRESSIONS FOR SPATIAL RESOLUTION

$$AR \approx \frac{Q}{4}\lambda$$

$$LR \approx 2.44\left(\frac{l_f}{D}\right)\lambda$$

distance, note that the beam shapes on both sides of the focal point are mirror images of one another, reflected about the focal plane. The beam behavior on one side of this plane, from the focus outward, has the same general characteristics that we earlier examined in Figure 5.17a for a beam propagating from an initially planar wavefront of a given diameter. Therefore, it stays approximately collimated within the transition distance z_R. Applied to the situation here, the transition distance of Equation (5.32) becomes

$$z_{R,d} = \frac{d^2}{4\lambda}$$

The depth of focus may be estimated to be twice this distance due to symmetry about the focal plane:

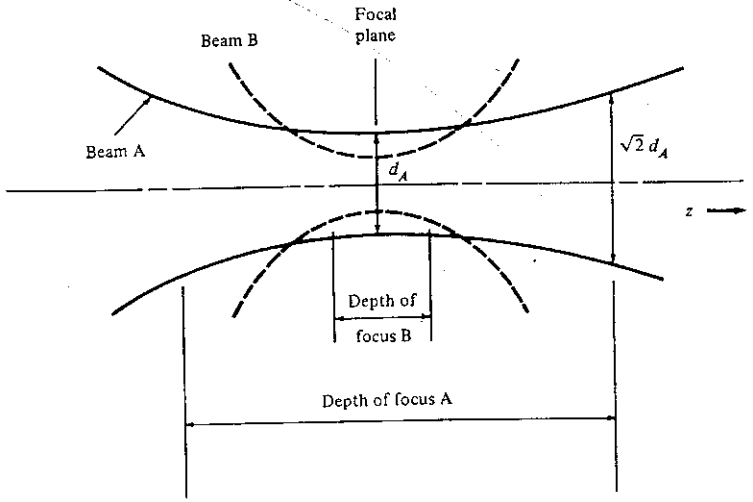

Figure 5.22 The depth of focus describes the longitudinal distance over which the beam maintains its approximate focused size. It gets shorter for tightly focused beams.

$$\text{Depth of focus} \approx \frac{d^2}{2\lambda} \approx 3\left(\frac{l_f}{D}\right)^2 \lambda \tag{5.55}$$

where Equation (5.51) was used to get the last result.

The tradeoff between focused size and depth of focus sometimes dictates a compromise in lens design. For example, in fixed-focus systems, the lens may be purposely given a nonspherical surface to cause the focused spot size to be larger than the theoretical limit, thereby increasing the depth of focus.

Example of Resolution Values

A numerical example of the spatial resolution limits for a typical medical ultrasound system is enlightening. The transducer pictured earlier in Figure 5.10 is designed for shallow cardiac imaging. It operates at 3.5 MHz with a Q of approximately 7. Its beam diameter is 1.5 cm and the focal length of the lens is 5 cm. Therefore, $\lambda = 0.043$ cm in tissue, and the theoretical resolution limits are

$$AR \approx \left(\frac{7}{4}\right)0.043 = 0.075 \quad \text{cm}$$

$$LR \approx 2.44\left(\frac{5}{1.5}\right)0.043 = 0.35 \quad \text{cm}$$

and depth of focus is approximately equal to 1.4 cm.

However, practical factors will worsen the lateral resolution. These factors include lens aberrations, objects being outside the depth of focus, side-lobe (or grating-lobe) off-axis sensitivity, spatial interference noise (speckle) due to the coherent nature of ultrasound, and signal compression in the receiver electronics. In addition, as mentioned in Section 5.2.2, practical factors such as dispersive absorption in tissue and signal compression in the receiver will degrade the axial resolution. Therefore, the actual resolutions are perhaps two to three times their theoretical values above. Note that, as is usually the case, the axial resolution is much better than the lateral resolution.

5.6 LINEAR ARRAYS

In real-time B-scanners, described in the next chapter, the transducer is sometimes composed of a linear array of closely spaced elements (usually

rectangular) as shown in Figure 5.23. Although each element may be small in terms of number of wavelengths, the overall width L can be appreciable (5 to 10 cm). The question is: What width is used in Equation (5.46) to calculate the angular divergence of the beam radiated from this unfocused transducer, the single-element width b or the overall-array width L? The answer depends upon whether the elements are excited one at a time or whether they are all radiating together.

If excited one at a time (as is done in the sequentially pulsed linear array machine), the pattern is, not surprisingly, just that of a single element; this pattern was covered in Figure 5.16b and is relatively broad in the horizontal direction, or azimuth, due to the smallness of the elements.

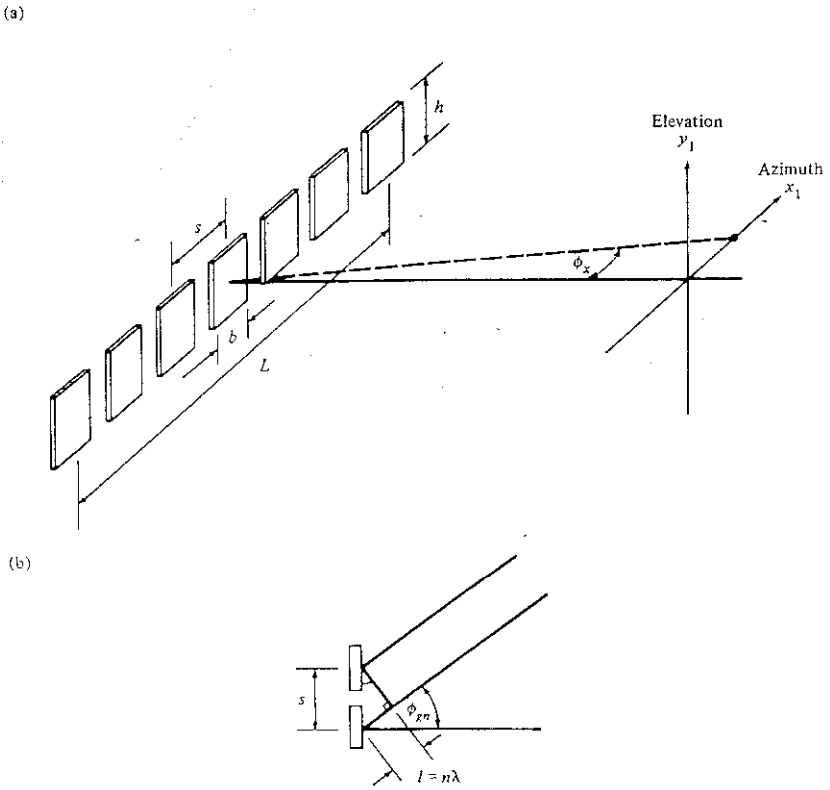

Figure 5.23 (a) The geometry for a linear array of rectangular elements. (b) A top view of two neighboring elements showing that at selected angles ϕ_{xn}, the path length difference l is equal to an integral number of wavelengths.

If the elements are excited simultaneously and coherently (as in the phased-array imager), the effective transducer width is L and the far-field divergence, given by Equation (5.46), will be much narrower. Correspondingly, if this coherent array is focused, the beam will converge to a smaller spot size with improved lateral resolution. (Note, however, that the beam divergence in the vertical direction, called the elevation, will be the same whether the elements are excited independently or coherently; in both cases the effective array height is h).

Grating Lobes

There is a complexity in the radiation pattern which accompanies the segmentation of the transducer into an array of elements. It is the appearance of reduced-amplitude images of the main beam (complete with side lobes) known as *grating lobes,* centered around one or more discrete angles in the ϕ_x plane. The angles of the grating lobes, denoted ϕ_{gn}, are found to be those angles for which rays from two neighboring elements are in phase with each other by a multiple of 2π; constructive interference therefore takes place at these angles, and some power is radiated in those directions. An alternate way of stating the condition for constructive interference is that the path length difference l between rays from the neighboring elements is equal to an integer number of wavelengths. Figure 5.23b shows that this occurs when

$$\sin \phi_{gn} = \frac{l}{s} = \frac{n\lambda}{s}$$

or

$$\boxed{\phi_{gn} = \sin^{-1}\left(\frac{n\lambda}{s}\right) \qquad n = \pm 1, \pm 2, \ldots} \tag{5.56}$$

There will be as many grating lobe orders in the pattern as the number of solutions of Equation (5.56) that fall within $\pm 90°$. Notice that, as the spacing s increases in size with respect to a wavelength, the grating lobes get closer together in angle and increase in number.

Figure 5.24 shows an example of a 16-element array with a total length of $L = 27\lambda$. Therefore, $s = (27/15)\lambda = 1.8\lambda$ and

$$\phi_{g1} = \pm 33.7°$$

Only the first-order grating lobes are present in this pattern since the second-order ($n = 2$) and higher-order lobes are not valid solutions (within $\pm 90°$) of Equation (5.56) for $s = 1.8\lambda$. The shape of the main beam and the displaced grating lobes is determined by applying Equation (5.45) with the

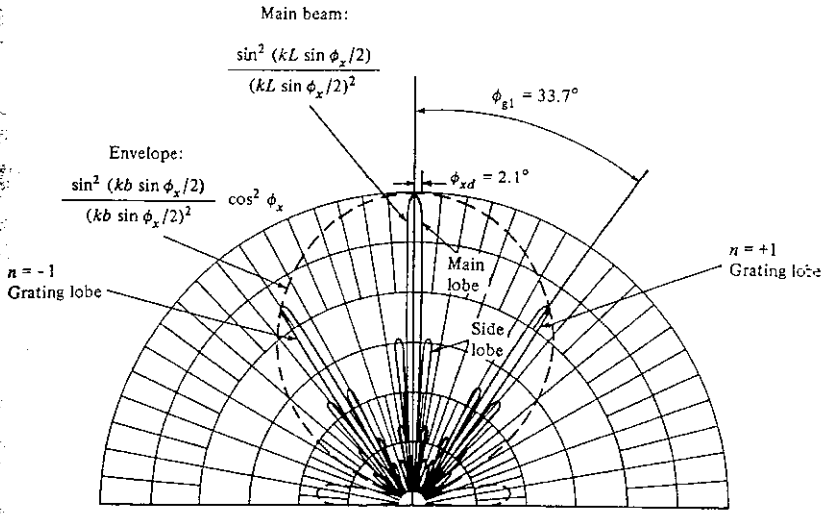

Figure 5.24 The power density beam pattern in the x_1 direction from a 16-element linear array whose elements are excited coherently. In addition to the main beam, copies of the main beam called grating lobes appear off to each side. For this example, $s = 1.8\lambda$ and $L = 27\lambda$.

effective length $b \to L$. Therefore, the width of the main lobe in the main beam (straight ahead) and also in the grating lobes is given by Equation (5.46):

$$\phi_{xd} = \sin^{-1}\left(\frac{\lambda}{L}\right) = \sin^{-1}\left(\frac{1}{27}\right) = 2.1°$$

The envelope which determines the amplitude of the grating lobes compared to the main beam is given by the directional factor H_r of one of the *individual* (assumed identical) elements, multiplied by a factor $\cos \phi_x$ (which is due to the lack of a reinforcing rigid baffle surrounding the elements and which has a major effect only near $\pm 90°$). Therefore, using Equation (5.45) for H_r,

$$\text{Envelope (amplitude)} = \frac{\sin[(kb \sin \phi_x)/2]}{(kb \sin \phi_x)/2} \cos \phi_x \tag{5.57}$$

since each element has a width of b (refer to Figure 5.23a). This envelope will possess zeros just like the main-beam directional factor, but they will be at much larger angles since $b \ll L$. The positions of the zeros of the envelope (in addition to $\pm 90°$ from the $\cos \phi_x$ term) may be obtained from Equation (5.46):

$$\phi_{xe} = \sin^{-1}\left(\frac{m\lambda}{b}\right) \qquad m = \pm 1, \pm 2, \ldots \tag{5.58}$$

Note that the closer to unity the ratio b/s is ("fill factor"), the closer the grating lobe angle from Equation (5.56) will be to a zero angle of the envelope from Equation (5.58), thus reducing the peak amplitude of the grating lobe. For the example of Figure 5.24, $b = 0.67s = 1.21\lambda$, and the envelope has the shape shown with zeros at $\pm 56°$.

An interesting envelope occurs for the special case of $s = 2b$ corresponding to a "square wave" array whose element's active width is just one-half the spacing between element centers. For this case, the angle of the second grating lobe

$$\phi_{g2} = \sin^{-1}\left(\frac{2\lambda}{s}\right) = \sin^{-1}\left(\frac{\lambda}{b}\right)$$

falls at the first zero in the envelope

$$\phi_{xe} = \sin^{-1}\left(\frac{\lambda}{b}\right)$$

and the second grating lobe essentially vanishes. In fact, all even-order grating lobes disappear, leaving only the main beam and odd-order grating lobes.

Grating Lobe Reduction

Reduction in the number and amplitude of the grating lobes is desirable since grating lobes represent potential sources of ambiguity in determining the direction of the echoes returned to the transducer. The principle of reciprocity applies under most circumstances to acoustic wave propagation, so the transducer's receiver sensitivity pattern will usually have the same shape as the transmitter radiation pattern. Therefore, grating lobes (and, to a lesser degree, side lobes) give off-axis sensitivity to a transducer used both as source and receiver. Reflecting points at the grating lobe angles are irradiated, and the receiver is sensitive to echoes coming from these angles in addition to straight ahead. Figure 5.25 shows how a single point scatterer will show up at three separate angular positions of a swept array with two grating lobes in addition to the main beam.

The angles of the grating lobes are governed by the spacing s between elements of the array, and their amplitude is determined by the envelope shape set by the individual element length b. In addition, the overall width L determines the angular width of each lobe, and the number of elements is given by $(L/s) + 1$. These array parameters can be manipulated by the

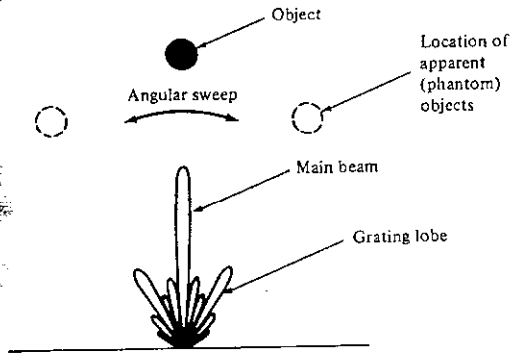

Figure 5.25 When the transducer is rotated, the grating lobes produce multiple responses from a single object, confusing the interpretation of object position.

designer to optimize one feature or another, depending upon the desired application, but they all interact. For example, to move the grating lobe angle as far away from 0° as possible, the spacing s between elements is made small. However, for a fixed number of elements, this reduces the array width L, which in turn *increases* the angular width of the main beam, worsening lateral resolution. Problem 5.22 gives other examples of the tradeoffs encountered in array design.

There is a temporal way to partially reduce the magnitude of the grating lobes in the transmitted pattern; it is based upon using very short transmitter pulses. As explained above, grating lobes are due to constructive interference occurring at selected angles between waves from neighboring elements. If the waves are really pulses of short duration (little more than one cycle), the pulse from one element propagating at the grating lobe angle will have decayed considerably by the time it is joined by the pulse from its neighbor, amounting to less than total constructive interference; this is diagrammed in Figure 5.26. When pulses from all the elements are considered, the skew in timing may significantly reduce the grating lobe response. The pattern in the forward direction remains essentially unaltered, however, since all pulses coincide in this direction, providing total constructive interference.

Thus, the ratio of grating lobe response to main lobe response decreases with decreasing pulse length (and therefore with decreasing transducer Q). For example, for a 16-element array with an interelement spacing of $b = 2.4\lambda$, the ratio of first grating lobe amplitude to main lobe amplitude is 0.2 when $Q = 9.4$ but only 0.08 when $Q = 3.1$. Unfortunately, this reduction in peak grating lobe response is accompanied by an increase in the angular width of the grating lobe.

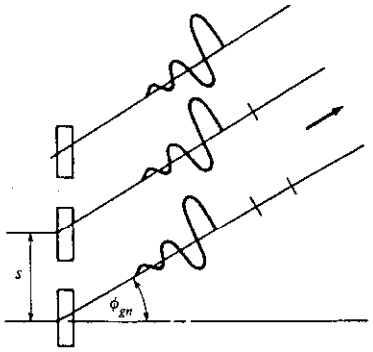

Figure 5.26 If short pulses are emitted from the elements of a linear array, their origins are skewed when summed at an angle. At the grating lobe angle ϕ_{gn}, some constructive interference takes place, but it is less than for continuous waves due to the decaying envelopes summed from neighboring pulses.

There is yet another way to attempt to reduce grating lobe response (for fixed L and for a given number of elements). The spacing between elements can be made nonuniform, defeating some of the constructive interference effects at off-axis propagation angles. This randomization of element spacing, however, is of minor benefit (especially for short pulses) and also increases the width of the grating lobe, so it is probably not worth the effort.

PROBLEMS

5.1. What is the thickness of a barium titanate transducer whose fundamental frequency of resonance is 5 MHz? How thick would it be if its third harmonic were 5 MHz?

5.2. A cw voltage with a peak magnitude of 10 V is impressed across a barium titanate transducer at its fundamental frequency of 1 MHz. The area of the transducer face is 1 cm^2. How much power is radiated into a layer of muscle in contact with the transducer?

5.3. Using the configuration shown in Figure 5.4, derive Equation (5.6) for the velocity of the transducer faces when excited at resonance by an electric field E_i. (*Hint:* Let the four traveling waves be displacement waves of the form

$$\xi_1 = A\cos(\omega t + kz)$$
$$\xi_2 = B\cos(\omega t - kz)$$
$$\xi_3 = C\cos(\omega t + k_1 z)$$
$$\xi_4 = D\cos(\omega t - k_2 z)$$

where ξ is the displacement of the material's particles from equilibrium and k, k_1, and k_2 are the propagation constants in the transducer, region 1, and region 2, respectively. Particle velocity u is given by $\partial\xi/\partial t$. Match particle velocity u and pressure p at each interface following the sign conventions

used in Section 3.4.2. The pressure just inside the transducer face is given by Equation (5.5) for a piezoelectric material. The net displacement inside the transducer (to calculate strain) is given by $\xi_1 + \xi_2$. Remember, at the frequency of fundamental resonance, $\lambda = 2l$ in the transducer, so $kl = \pi$. Solve for $u_f = -\omega D \sin(\omega t - k_2 l)$.

5.4. Use Equation (5.12) to solve for the equivalent electrical circuit of an air-backed transducer at resonance. Procedure: Substitute Equation (5.5) into Equation (5.12), then integrate with respect to z from $z = 0$ to $z = l$. The integral of electric field is voltage ($V = \int E_i\, dz$) and let σ_i be a constant. Solve for the total charge $q = A\sigma_i$ in terms of V and the displacements ξ of the two faces. Then, find the current $I = dq/dt$. Here, you will need to remember that $d\xi/dt = u_f$ of the faces (given by Equation (5.6) with opposite signs for the two faces) and let $V = \hat{V}\cos\omega t$, so $E_i = (V\cos\omega t)/l$. The electrical admittance is finally given by I/V. Show that the admittance is the sum of two parts, one due to a capacitance with an admittance of magnitude ωC_0 (90° out of phase from V), and the other due to a resistor with admittance $1/R_m$ (in phase with V). Check your answers for C_0 and R_m with Equations (5.16) and (5.17).

5.5. An air-backed PZT transducer is radiating into water at its fundamental resonant frequency of 3 MHz. It has a surface area of 5 cm^2. Find its equivalent electrical circuit, including values for the components (assume it is internally lossless). When driven with a sinusoidal peak voltage of 10 V, use R_m to calculate how much power is radiated by this transducer.

5.6. Using Figure 5.9, derive Equation (5.24) for axial resolution. Find an approximate numerical value (including units) for the axial resolution of a bioinstrument whose transducer has a frequency $f_1 = 2.25$ MHz and a $Q = 5$.

5.7. (a) Find the approximate Q of the following quartz transducer arrangement at its fundamental frequency of 2 MHz by using Equation (5.18):

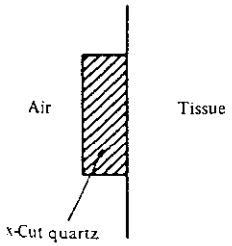

Assume that the internal losses of the transducer are zero, so that losses are due entirely to the transmission of power through the transducer faces. (*Hint:* Assume an internal wave with intensity I_0 is bouncing back and forth between the faces. Determine how much intensity is lost during one period of the fundamental frequency. Let the stored intensity be an average of before and after the bounces.)

(b) Calculate the axial resolution for this quartz transducer.

5.8. To investigate the reasons for adding an absorber to the back face of a transducer, redo Problem 5.7 for the same frequency and quartz material, but replace the air with a backing material made of an absorber whose acoustic impedance $Z = 3 \times 10^6$ kg/m^2 s is closer to quartz. Assume that all power radiated into the absorber is lost. Find the new Q and the axial resolution.

5.9. Redo Problem 5.7 for the same frequency and *air* backing, but use PVDF as the transducer material instead of quartz. What are the Q and the axial resolution now?

5.10. Applying the method outlined in Problem 5.7 to a general transducer with impedance Z_c radiating on one side only into a medium with impedance Z_2, show that an approximate expression for the transducer's Q at its fundamental frequency is given by

$$Q \approx \frac{Z_c \pi}{2Z_2}$$

when $Z_c \gg Z_2$.

5.11. Using geometry in Figure 5.11, show that r' is given by Equation (5.26).

5.12. Derive Equation (5.30) for the on-axis pressure field of a circular transducer starting from Equation (5.29) and following the steps outlined in the text.

5.13. Derive Equation (5.37) from Equation (5.36) using the integral relationship between J_0 and J_1 given in the text.

5.14. Integrate Equation (5.34) over a rectangular source of dimensions $b \times h$ using the geometry shown in Figure 5.16a to get the pressure radiation pattern of Equation (5.44) along the x_1 axis.

5.15. (a) Plot the pattern (similar to Figure 5.15a) of intensity measured on a plane 50 cm away from a 2-MHz unfocused circular transducer whose diameter is 1 inch. Find the diameter of the closest null ring surrounding the central peak of the pattern.

(b) Estimate the FWHM diameter of the central peak as given by the width to the −3-dB points on either side of the peak.

5.16. Find the near-field to far-field transition distance and the far-field divergence angle for each of the unfocused transducers listed below:

(a) Diam. = 1 cm, frequency = 1 MHz

(b) Diam. = 3 cm, frequency = 1 MHz

(c) Diam. = 1 cm, frequency = 2.25 MHz

5.17. An unfocused circular transducer is used in the following configuration at a frequency of 3 MHz:

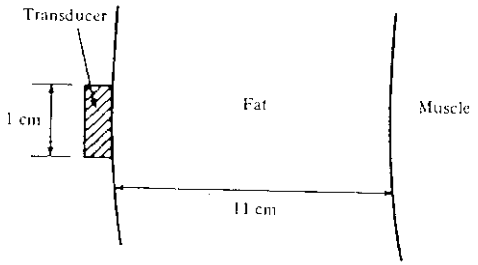

Estimate the power which the transducer must radiate into the tissue in order to receive 2×10^{-8} W back at its face from the echo due to the fat/muscle interface. Include the effects of *beam spreading* and list any simplifying assumptions you make.

5.18. Use Snell's law and ray racing to show that the focal length of a plano-concave lens is given by Equation (5.48). (*Hint:* Consider a ray entering parallel to the axis and use the small-angle approximation to find the distance where it intersects the axis.)

5.19. How large a diameter would a focused circular transducer of frequency 1.5 MHz have to be to give a focused spot size of 1 mm at a distance of 10 cm from the transducer? What would be the depth of focus of this beam?

5.20. Find the theoretical axial resolution and lateral resolution at a distance of 6 cm from a circular *unfocused* transducer whose frequency is 3 MHz, whose diameter is 1.5 cm, and whose Q is 10.

5.21. In echocardiography it is desirable to image the mitral valve leaflets with a resolution of approximately 2 mm. The distance from the chest wall to the valve is about 7 cm. To avoid excessive attenuation, a frequency of 2.25 MHz is used.

(a) Determine the maximum Q allowed for the transducer which will give the required resolution.

(b) Determine the minimum diameter of the lens (and therefore the transducer) which will give the required resolution, assuming focusing on the valve.

5.22. (a) Sketch a rough polar power density plot for a coherently excited linear array composed of 16 square elements, each 1 mm wide with a center-to-center spacing of 2 mm. The frequency is 2.25 MHz. Calculate the following three important features: width of main lobe; angular positions of the grating lobe(s); and ratio of peak power density in first grating lobe to peak power density in main lobe.

(b) Explain qualitatively how each of the above three pattern features would change if each of the following modification was made independently in the array (all other parameters stay as specified):

(i) The wavelength was decreased.

(ii) The spacing between elements was decreased.

(iii) The number of elements was decreased to eight.